Pre-normative REsearch for Safe use of Liquid Hydrogen (PRESLHY)

Project Deliverable

Theory and Analysis of Combustion of Pre-mixed systems with cryogenic hydrogen

Deliverable Number:	D5.1
Work Package:	5
Version:	7.1
Author(s), Institution(s):	Mike Kuznetsov, KIT
Submission Date:	30 November 2020
Due Date:	30 June 2019
Report Classification:	Public

This project has received funding from the Fuel Cells and Hydrogen 2 Joint Undertaking under the European Union's Horizon 2020 research and innovation programme under grant agreement No 779613.

History		
Nr.	Date	Changes/Author
1.0 - Draft	1.11.2019	Draft version by Mike Kuznetsov
4.0 - Draft	9.3.2020	Review version
7.0	26.11.2020	Integrating all revision comments
7.1	2.10.2018	Cover page and summary added, uploaded

Approvals			
Version	Name	Organisation	Date
4.0 - Draft	Simon Coldrick	HSE	1 July 2020
4.0 - Draft	Thomas Jordan	KIT	1. June 2020

Acknowledgements

This project has received funding from the Fuel Cells and Hydrogen 2 Joint Undertaking under the European Union's Horizon 2020 research and innovation programme under grant agreement No 779613.

Disclaimer

Publishable summary

A literature survey and analysis of existing experimental data on cryogenic hydrogen combustion has been done. It includes different phenomena associated with accident scenarios involving LH2 as a fuel and ambient air as an oxidizer. The phenomena include LH2 jet fire behaviour, its scaling and radiation properties; burning LH2 pool behaviour, radiation characteristics; cryogenic hydrogen combustion in a layer geometry relevant to flame spread over the spill of LH2; flame acceleration and deflagration-detonation-transition for cryogenic hydrogen-air clouds in an enclosure; LH2 combustion in an enclosure. BLEVE processes are not included in the analysis because of the planned contribution from SH2IFT project. Major characteristics of combustion characteristics are evaluated from existing experimental data or extrapolated and theoretically predicted in cases of the lack of data. The knowledge gaps for different phenomena are defined and the main tasks for the forthcoming experiments are formulated.

Key words

Liquid hydrogen, jet fire, flame acceleration, DDT, pool fire, BLEVE, thermal radiation, harm, safety distances

Abbreviations

LH2	Liquid Hydrogen
LOX	Liquid Oxygen
LN2	Liquid Nitrogen
BR	Blockage Ratio
LFL	Lower Flammability Limit
UFL	Upper Flammability Limit
FA	Flame Acceleration
DDT	Deflagration – to – Detonation Transition
MIE	Minimum Ignition Energy
LNG	Liquid Natural Gas
LPG	Liquid Petroleum Gas
SEP	Surface Emissive Power

Table of Contents

1. Introduction (KIT)

The theory of cryogenic hydrogen combustion is based on general theory of combustion with a difference that the state of combustible matter can be condensed, two-phase or gaseous but in all the cases at least non-ideal and the real gas equation of state (RG EoS) should be used. Independent of how low the cryogenic temperature is, the danger of cryogenic hydrogen combustion could be stronger than hydrogen combustion at ambient temperature and pressure because of 5-10 times higher density of combustible matters. How the density factor balances against the lower hydrogen reactivity at cryogenic temperatures is of great practical importance.

According to the literature survey, theory and existing experimental data analysis a lot of knowledge gaps in understanding of related physical phenomena can be specified in order to be solved and be closed by numerical modeling and experiments. The strategy for modeling and numerical simulations should be oriented to the problem, how to validate theoretical models against the new and existing experimental data. The feedback between experimental results and recent models and simulations should then lead to a better understanding of the process, the capability to predict characteristics of the processes for LH2 combustion, and produce a set of simplified engineering correlations to predict the hazards of LH2 combustion.

Special attention should be paid to the following specific problems relevant to cryogenic temperature combustion:

- Combustion under cryogenic temperatures, at the conditions of the very dense real gas state, close to condensed phase density. Being ignited, combustion products behave as an ideal gas.
- Heterogeneous combustion in the presence of condensed (liquid or solid) oxygen, nitrogen, CO2 and H2O. Thus, instead of a volumetric process, a chemical reaction at the surface (liquid or solid) may occur.
- Effect of cryogenic temperatures on thermodynamics and kinetics of combustion process leading to several times lower speed of sound and viscosity of the gas. The major problem here is that existing thermodynamic databases are tabulated up to 200K as the lowest temperature with non-confidential extrapolation until 100K. Chemical kinetics exists in the temperature range above 300K with the non-validated assumption that the reaction rate will be governed by the same activation energy at cryogenic temperatures.
- Simultaneous combustion and phase transition (flush evaporation) of hydrogen above the spill of LH2.
- Effect of the inverse hydrogen concentration gradient (higher hydrogen concentration at the ground level) on combustion dynamics in a layer geometry.
- Radiation characteristics of LH2 combustion.

The main objectives of this work are the following: (1) to complete the experimental database on cryogenic LH2 combustion, including laminar and turbulent combustion and detonation of premixed and stratified hydrogen compositions with air at cryogenic temperatures; (2) to analyze experimental data in order to develop and validate existing or generate new models for LH2 combustion; and (3) to develop empirical and semi-empirical engineering correlations for practical applications.

At the starting point of this project the following list of LH2 specific combustion phenomena was considered to be addressed:

- LH2 jet fire behaviour, including scaling and radiation properties
- Stationary burning LH2 pool behaviour, radiation characteristics.
- Cryogenic hydrogen combustion in a layer geometry relevant to flame spread over the spill of LH2
- Flame acceleration and deflagration-detonation-transition for cryogenic hydrogen-air clouds in an enclosure.
- BLEVE process with pressurized or non-pressurized LH2.[1]
- LH2 combustion in an enclosure. Effects of pressure, temperature, heat radiation, convection, geometry, congestion, pressure peaking, etc.

2. Initial conditions. Real gas equation of state (KIT)

Since in reality the combustion process of liquid hydrogen and ambient air occurs only in the gas phase the temperature range set by LH2 temperature of 20.28K to the ambient temperature of air of 300K may be reduced for further investigations.

For instance, the calculations with NIST data base [NIST JANAF Thermochemical Tables (1985)] for 1 bar of ambient pressure gives the lowest temperature T_L for gaseous hydrogen-air composition in whole range of hydrogen concentrations from 0 to 99%H2 (Figure 1).

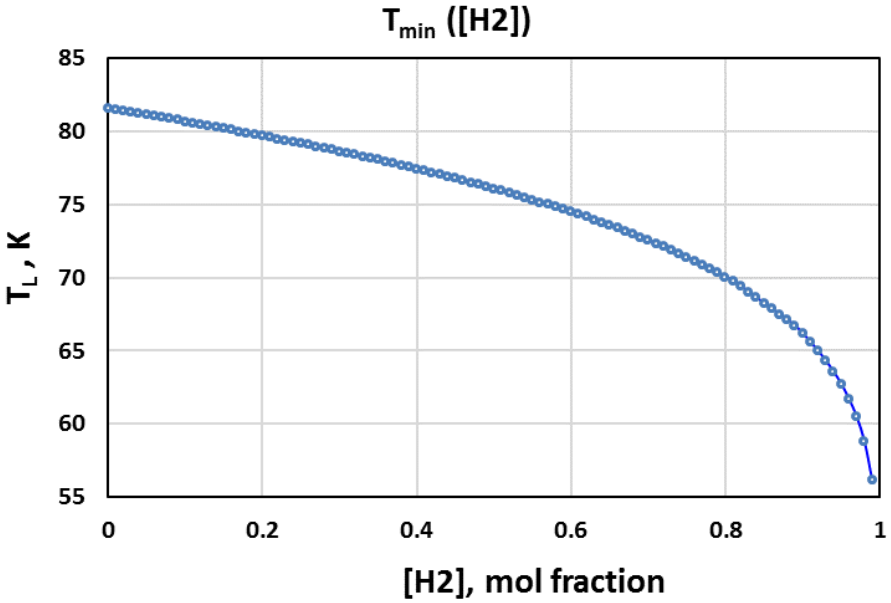

Figure 1. Saturation temperature for liquid phase transition for hydrogen-air mixtures (1 bar).

Homogeneous gaseous reactions will only occur above the saturation temperature T_L. The picture shows that within the standard flammability limits (4-75%H2) the lowest temperature changes from 71.4K (at UFL = 75%H2) to 81.2K (at LFL = 4%H2). This means that almost full range of burnable hydrogen-air compositions (above 16%H2) is

[1] Because of budget limitations the BLEVE will not be experimentally investigated in PRESLHY. Instead, a close cooperation with the Norwegian project SH2IFT is envisaged, where tests for BLEVE will be conducted

located above 80K. Such temperature can easily be achieved by liquid nitrogen cooling system. The non-ideality of the gas is rather small at such conditions (>80K, 1 bar). The compressibility factor changes from 0.99 to 0.96. Thus the existing thermodynamic JANAF tables can be easily extended at least up to 80K. At such a temperature, the real gas density is only 0.5 to 4% higher than the ideal gas density. Nevertheless, the density difference should be taken into account for calculations of expansion ratio for combustion products, σ:

$$\sigma = \frac{\rho_u}{\rho_b}, \quad (1)$$

where ρ_u is the fresh (unburnt) gas density; ρ_b is the combustion products density. The low temperature affects the reaction rate on one side and the densities of the involved gases (4 times higher at 80 K than at standard conditions) on the other side. The problem is that chemistry in general and chemical reaction mechanisms cannot be extrapolated to such low cryogenic temperatures compared to thermodynamics. At least all mechanisms should be validated against experiments. There are some papers [Faisal Khan et al., 2013] demonstrated a capability to use within FLUENT code the well known H2/O2 mechanism [Burke et al., 2012] to cryogenic temperatures. The authors [G. Ribert et al., 2008] also implemented a known mechanism by Li et al. (2004) to calculate counter flow hydrogen-oxygen flames at the low temperature of 100K. An overview of low temperature chemistry for hydrocarbons and hydrogen can be found in Klotzbücher W.E. (1987).

Taking into account liquefaction of air components at cryogenic temperatures, the actual temperature range can be chosen for forthcoming experiments on the base of real gas state using NIST thermodynamic tables. Table 1 shows the lowest temperatures required for flammable conditions (4-75%H2) of hydrogen-air compositions. Note "St" corresponds to the stoichiometric concentration of hydrogen in air. It follows from the table that at 1 bar the initial temperature has to be higher than 81K. At 0.5 bar the lowest experimental temperature for uniform gaseous compositions can be reduced to 75.8K (below liquid nitrogen temperature).

Table 1 The lowest temperature T_L for flammable concentrations of hydrogen-air mixtures (using NIST database)

T_L, K	P, bar	%O2 max	%H2	Note
71.4	1	5.25	75	UFL
78.6	1	14.7	30	St
81.2	1	20.2	4	LFL
67.4	0.5	5.25	75	UFL
73.6	0.5	14.7	30	St
75.8	0.5	20.2	4	LFL

At temperatures lower than T_L, a two-phase system of the gaseous hydrogen-air mixture and a liquid oxygen+nitrogen coexist. The liquid phase will be more than 10 times enriched with oxygen as compared with the gaseous part, where the ratio of oxygen to nitrogen is fixed as 1:3.76. In a liquid, the ratio of O2/N2 is changing from 1:0.92 at 81.6K to 1:0.29 at 56.17K. The solubility of hydrogen in liquid substance is negligibly small at such temperatures and reaction may only take place at the interface gas – liquid. The efficiency of such a reaction is very small due to a limited reaction surface and also a very low diffusion of oxidizer in a liquid phase. Another problem is that there are no proper

mechanisms and reaction rates between gaseous hydrogen and liquid oxygen. However, the paper Faisal Khan et al. (2013) shows a success to extend the well known chemistry developed at normal initial conditions to the temperature of LH2.

If the temperature approaches 20.27K of liquid hydrogen then, at the temperature below 63.1K for nitrogen and below 54.36 for oxygen, a solid phase appears. The probability of reaction between gaseous hydrogen and solid oxygen can even be higher due to absorption of hydrogen at solid surface which is significantly larger than the liquid one. Additionally, the reaction can be activated due to the heat of absorption. Exactly at the interface LH2 – solid oxygen, the reaction liquid fuel – solid oxidizer may occur. It should be like high explosive reaction due to the extremely high energy density of the system. The only problem is that reaction should be activated due to some exothermic process similar to friction, spark, electrostatic discharge, shock wave or something else local leading to energy release.

The mixture LH_2/solid oxygen is well known as a high explosive. Rico (1970) theoretically and experimentally studied the mixture LH_2/solid oxygen. Detonation pressure P_{CJ} = 27000 – 31000 bar and detonation velocity D = 5000 - 8250 m/s were theoretically predicted and then measured. Similar to high explosives, mixtures of solid oxygen in excess (with respect to stoichiometry) and LH2 are shock sensitive (NASA report 1740.16, 1997). A local shock equal to 100 MPa may lead to the detonation of such composition.

The secondary explosion of a solid oxygen “cake” formed on top of LH2 pool occurred during HSL experiments (Hall et al., 2014). The reason of such an explosion is not clear yet.

References

Burke, Michael P., Marcos Chaos, Yiguang Ju, Frederick L. Dryer, Stephen J. Klippenstein, Comprehensive H2/O2 kinetic model for high-pressure combustion, International Journal of Chemical Kinetics (2012) 44(7): 444-474

Chase, M.W., Jr., C.A. Davies, J.R. Downey, Jr., D.J. Frurip, R.A. McDonald, and A.N. Syverud, NIST JANAF Thermochemical Tables (1985) National Institute of Standards and Technology Gaithersburg, MD 20899

Faisal Khan, Dr Ugur Guven, Zeya Ahmad Quadri, CFD simulation of a liquid rocket propellant (LH2/LOX) combustion chamber, Proc. Of the 15th Annual CFD Symposium, Indian Institute of Science, August 9-10, 2013, Bangalore, pp. 1-9

Guillaume Ribert, Nan Zong, Vigor Yang, Laetitia Pons, Nasser Darabiha , Sébastien Candel, Counter flow diffusion flames of general fluids: Oxygen/hydrogen mixtures, Combustion and Flame, 154 (2008) 319 - 330

Hall, J.E., P. Hooker, D. Willoughby, Ignited releases of liquid hydrogen: Safety considerations of thermal and overpressure effects, International Journal of Hydrogen Energy, Volume 39, Issue 35, 2014, Pages 20547-20553

Klotzbücher W.E. (1987) Low Temperature Chemistry. In: Sinclair C. (eds) The Status of Soviet Civil Science. Springer, Dordrecht

Li, J., Z. Zhao, A. Kazakov, F.L. Dryer, An updated comprehensive kinetic model of hydrogen combustion, Int. J. Chem. Kinet., 36 (2004), pp. 566-575

National Aeronautics and Space Administration Report, Safety Standard for Hydrogenand Hydrogen Systems, Report NSS 1740.16, 1997, p. A-16

Rico Hubert Yves, Etudes théorique et expérimentale de la détonation des mélanges d'hydrogène liquide et d'oxygène solide à 20 K Thèse de doctorat de l'Université de Paris 1970

3. Fundamental combustion properties (KIT)

Flammability limits, ignition time delay, minimum ignition energy, laminar flame velocity, expansion ratio are the fundamental combustion properties based on thermodynamics and chemical kinetics. Some of them (thermodynamics based), such as expansion ratio, maximum combustion pressure and temperature, can be calculated from first principles with a correction to the real gas equation of state approaching to liquefaction temperature T_L. Most of them (chemical kinetics based), such as laminar flame velocity, flammability limits, minimum ignition energy, can be evaluated experimentally within a certain range of temperatures with a very accurate extrapolation to cryogenic temperatures with a strong need to experimentally validate extrapolation afterward. Usually, those properties do not depend on the geometry of the system and its scale and can be *a priori* used as a measure of chemical reactivity.

3.1. Flammability limits

There exists a range of fuel concentrations, from lean to rich limit between that different flame propagation regimes can be occurred. Beyond this range, the flame will not propagate for a long distance from an ignition source. There are several European and American standards for flammability limits. The European one (prEN 1839 „B“) is based on 5% combustion pressure exceed of ignition spark pressure in pure air. The American standard is based on flame detachment from ignition source and some distant propagation. In principle, the term "flame propagation" is very conventional. For instance, Kumar (1985) proposed that a mixture was assumed to be flammable if the flame front was detected in the whole test volume (not less than 1.2 m as proposed US Bureau of Mines), regardless of how the flame was produced. If the flame travels some distance from the ignition source, and then the flame quenches, the mixture can be indicated in this case as non-flammable one. Such a method allows to use very powerful ignition source assuming that the far traveling of the flame is a criterion of stable flame propagation without an influence of ignition source energy. However, a very big difference in standards leads to a difference in flammability limits. To minimize the difference, the ignition source energy should be limited by the values of 5-6 J.

Table 2 Flammability limits at low temperatures (Wierzba et al., 1992)

Initial temperature (°C)	Lean flammability limit (H2 %vol)	Rich flammability limit (H2 %vol)
0	-	72.7
-30	4.0	72.0
-60	4.1	71.2
-100	4.3	-

Wierzba et al (1992) studied the influence of low temperature on upward flammability limits in a stainless steel smooth circular tube of 50 mm diameter and 1 m in length. Ignition of the test mixture was obtained by an electric spark discharge between two horizontal conical tungsten electrodes that were spaced 6.5 mm apart and centered in the tube 35 mm from the lower end of the tube. As shown in Table 2, the flammability domain is slightly

reduced at lower temperatures. The data do not cover the cryogenic temperatures but at least it shows a trend to reduction of flammable domain with temperature decrease.

Quite different results at lower temperatures up to – 130°C using the same experimental facility obtained by Karim et al. (1984). The data show a stronger shrinking of flammability limits at cryogenic temperatures (Table 3).

Table 3 Flammability limits at low temperatures (Karim et al., 1984)

Initial temperature (K)	143	186	218	246	273	298
Lean flammability limit (H2 %vol)	6.21	5.66	5.24	4.88	4.52	4.13

It has to be also noticed that the influence of low temperature on horizontal and downward flammability is not available in the literature.

The data on flammability limits at low temperatures (Karim et al., 1984 and Wierzba et al., 1992) fit very well to the data at ambient and elevated temperatures up to 400 ºC obtained in different papers (Gasse, 1992 [4]; Kumar, 1985 [5]; Hustad et al., 1988 [6]; DeSoete, 1975[7] in Figure 2). Figure 2 includes experimental data on flammability and self-ignition limits experimental (Zabetakis, 1965[14]) and calculated (Kuznetsov et al., 2008; Kuznetsov et al., 2013) in a whole range of temperatures and concentrations for hydrogen – air mixtures at ambient pressure. The domain below the self-ignition limit and between the lower and upper flammability limits corresponds to flammable mixtures area ignited by an external ignition source (spark, glow plug, hot surface)

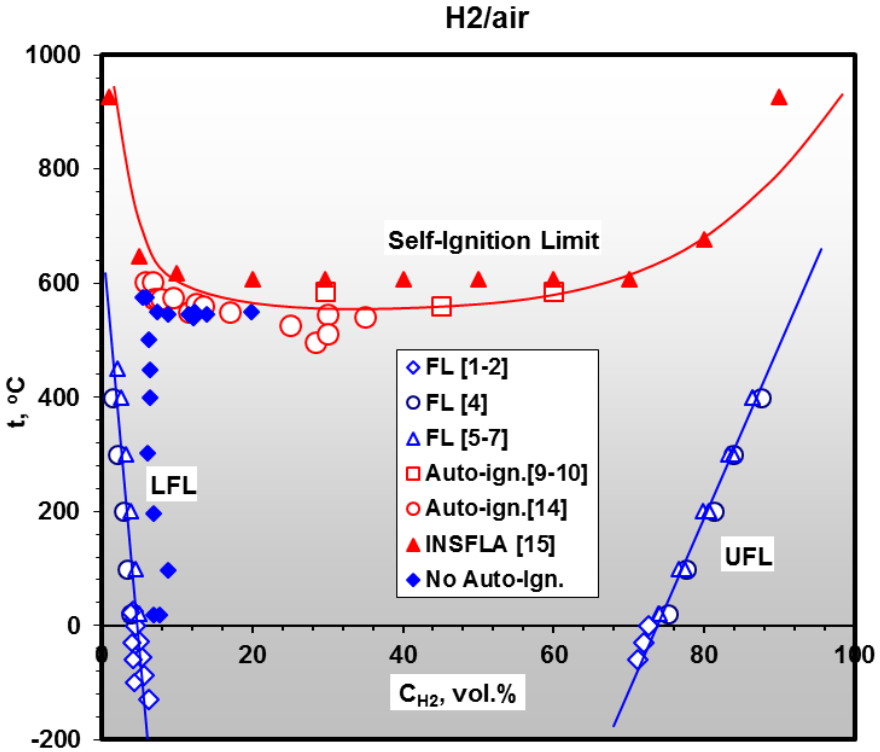

Figure 2. Flammability and self-ignition limits for hydrogen-air mixtures at different temperatures.

Figure 2 shows a well linear dependence of flammability limits against temperature which corresponds to so called Burgess-Wheeler law. To describe data in Table 2 the authors (Wierzba et al., 1992) propose a linear interpolation of the LFL at the temperatures 150-300 K as follows:

$$\frac{C_{LFL}(T)}{C_{LFL}(T_0)} = 1 - 0.000721 \cdot (T - T_0) \tag{2}$$

where $C_{LFL}(T)$ and $C_{LFL}(T_0)$ are the lower flammability limits at given temperature T with unknown minimum hydrogen concentration and at the reference temperature T_0 with known LFL. A similar correlation was developed (Wierzba et al., 1992) for upper flammability limit (UFL) for rich hydrogen-air mixtures:

$$\frac{C_{UFL}(T)}{C_{UFL}(T_0)} = 1 + 0.000721(T - T_0), \tag{3}$$

where $C_{UFL}(T)$ and $C_{UFL}(T_0)$ are the lower flammability limits at given temperature T with unknown minimum hydrogen concentration and at the reference temperature T_0 with known UFL.

Zabetakis (1965) used this dependence easier in the form:

$$C_{LFL}[vol.\%] = 4.13 - 0.013 \cdot (t - 25^{o}C), \tag{4}$$

where C_{LFL} is unknown lower flammability limit for a given temperature t [ºC] relatively to the lower flammability limit C_{LFL} = 4.14 vol. %H_2 at the ambient temperature t = 25 ºC. Zabetakis (1965) extrapolated correlation Eq. (4) until LH2 temperature and obtained the value C_{LFL} = 7.7 vol. %H_2.

For the temperatures higher than 300 K Baker et al. (1978) propose a linear dependence as follows:

$$C_{LFL}[vol.\%] = 4.0 - (T - 300)/121.61, \tag{5}$$

where C_{LFL} is unknown lower flammability limit for a given temperature T [K] relatively the lower flammability limit C_{LFL} = 4.0 vol. %H_2 at the ambient temperature T = 300 K. Summarizing all the experimental in the range -150 – 400 [ºC] for the practical application we recommend to use a linear interpolation:

$$C_{LFL}[vol.\%] = 4.397 - 0.0063t[\mathrm{oC}], \tag{6}$$

where C_{LFL} is unknown lower flammability limit for a given temperature t [ºC] relatively the lower flammability limit C_{LFL} = 4.397 vol. %H_2 at the temperature t = 0 ºC. At ambient temperature t = 20 ºC Eq. (6) gives a little bit higher value of C_{LFL} = 4.27%H2 than measured but the correlation covers a wide range of temperatures.

Experimental data of (Gasse, 1992; Kumar, 1985; Hustad, 1988; DeSoete, 1975) on upper flammability limits (UFL) for hydrogen-air mixtures in the temperature range 20-400 ºC are presented in Figure 2. Baker et al. (1978) propose a linear dependence for UFL as follows:

$$C_{UFL}[vol.\%] = 74.0 - (T - 300)/37.85, \tag{7}$$

where C_{LFL} is unknown upper flammability limit for a given temperature T [K] relatively the upper flammability limit C_{UFL} = 74.0 vol. %H_2 at the ambient temperature T = 300 K. Summarizing all the experimental in the range -60 – +400 [^oC] for the practical application in order to calculate the upper flammability limits (UFL) we recommend to use a linear interpolation:

$$C_{UFL}[vol.\%] = 73.8 + 0.033 \cdot t[^oC], \quad (8)$$

where C_{UFL} is unknown upper flammability limit for a given temperature t [^oC] relatively the upper flammability limit C_{UFL} = 73.8 vol. %H_2 at the ambient temperature t = 0 ^oC. Blue solid lines corresponding to the linear dependencies Eqs. (6) and (8) extrapolated to the highest temperatures above 600 ^oC are shown in Figure 2 and demonstrate good agreement between all experimental data and proposed correlations.

The flammability limits correlations as a function of initial temperature proposed for stagnant initial conditions. Of course, in a real accident scenario, in presence of overlapping effects of elevated pressure and flow velocity under high pressure hydrogen releases the ignitability of a non-uniform turbulent hydrogen jet can be significantly changed. The ignition and combustion characteristics of such a gasdynamic structure as a hydrogen jet will be one of the major goals of the ongoing PRESLHY project.

3.2. Minimum Ignition energy (MIE)

The minimum ignition energy (MIE) is one of the most important characteristics of chemical reactivity and combustion energy for flammable mixtures. According to Lewis and von Elbe (1987) to ignite a mixture, the spark should provide an appropriate amount of energy within a critical size similar to that for the burnt mixture itself. The MIE is influenced by the mixture's initial temperature because of density changes. To our knowledge, there is no publication on the influence of low cryogenic temperature on the MIE of hydrogen-air mixtures. At least, according to the theoretical equation (Lewis, von Elbe, 1987) the minimum ignition energy H should decrease with initial temperature decrease:

$$H = \frac{\pi d^3}{4} K C_p \rho_u T_u \left(1 - {}^{T_u}/_{T_b}\right), \quad (9)$$

Where d is the quenching distance; K is the stretch factor (K = 0.5 for stoichiometric hydrogen-air); C_p is the heat capacity; ρ_u is the initial density of the mixture; T_u is the initial temperature of unburned material; T_b is the adiabatic combustion temperature. In Lewis and von Elbe (1987) work the MIE for stoichiometric hydrogen-air mixture changes linearly from 31.5μJ to 18μJ with the initial temperature increase from 0 ^oC to 100 ^oC. The data fit well to the correlation

$$E_{min}[\mu J] = 31.44 - 0.1346t[oC], \quad (10)$$

The same behaviour was found by Gan Cui et al. (2016) for methane-air at different pressures, the MIE increases with a decrease of the initial temperature to cryogenic temperatures. The MIE increases from 0.5 mJ to 1.3 mJ with a temperature decay from 273 to 123 K (Figure 3). Similar behaviour can probably be expected for hydrogen-air mixtures at low and cryogenic temperatures.

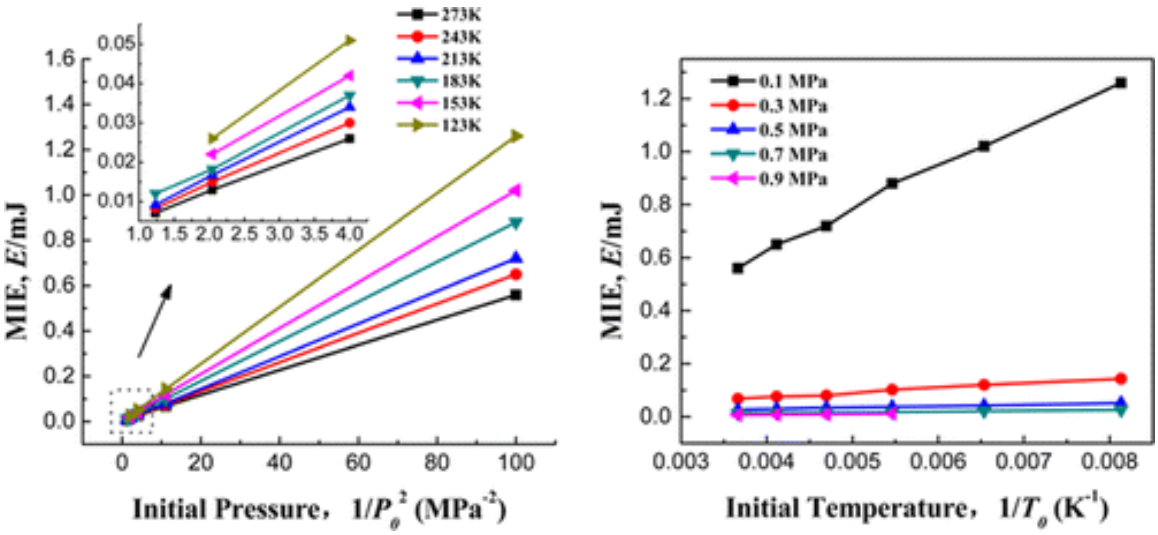

Figure 3. Pressure (left) and temperature (right) dependences of MIE for methane-air mixture.

It was found that a semi-empirical correlation obtained up to 200K by Martín-Valdepeñas et al. (2003) for stoichiometric, lean and rich hydrogen-air compositions can be used even up to cryogenic temperatures. Figure 4 shows the same trend as methane-air (Figure 3) and hydrogen-air mixtures at elevated temperatures (Eq. 10). The Minimum ignition energy increases with the initial temperature decrease within the cryogenic domain. The picture also shows a strong MIE increase for lean and rich hydrogen – air mixtures in comparison with stoichiometric one. The difference takes one or two orders of magnitude. For some reasons, the data by Valdepeñas et al. (2003) give two times higher MIE than given by Lewis and von Elbe (1987).

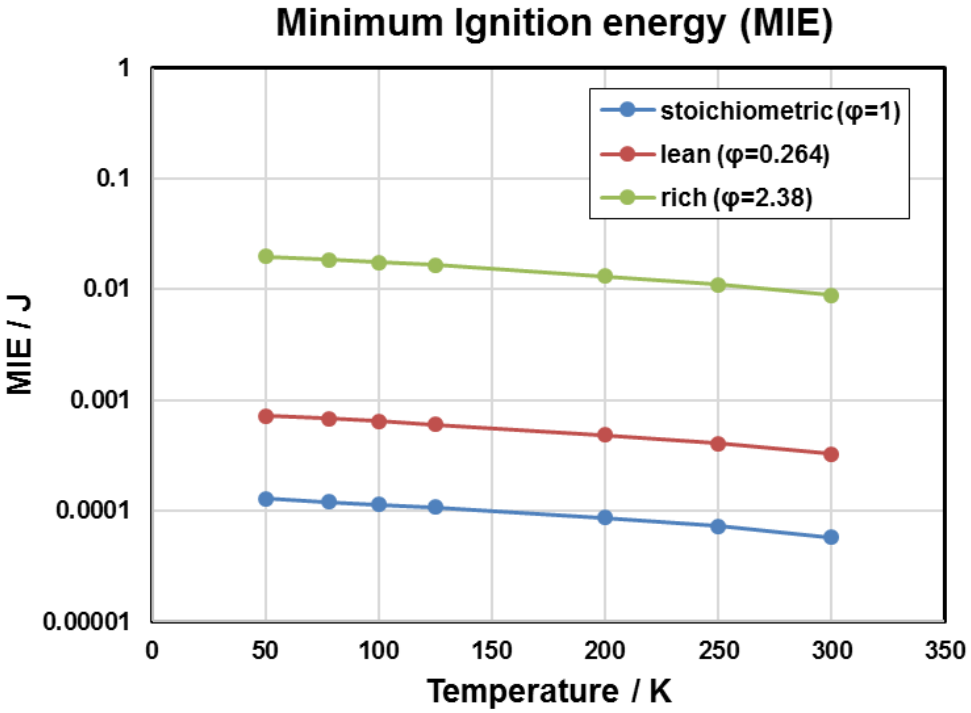

Figure 4.Minimum Ignition Energy as function of initial temperature.

3.3. Laminar flame speed

The laminar flame speed is one of the most important integral characteristics of the chemical reactivity of combustible mixtures. Using a spherical bomb and the pressure trends, Bavoil (1997) studied the influence of cold initial temperature on the laminar flame speed of H2/air mixtures from 100 to 300K for different equivalence ratios (Rich on the figure). For equivalence ratio (Richesse in French) he proposed values of alpha to calculate the laminar flame speed in low temperature conditions.

In explosion science, in many situations the flame speed V_f is (at least at the beginning of the flame propagation) proportional to the product of the expansion ratio with the laminar flame speed. At ambient conditions, V_f = 6.89 * 2.1 = 14.47 m/s. At 100 K, V_f = 20 * 0.4 = 8 m/s. On this basis, cryogenic conditions could be considered as less reactive than ambient conditions.

According to the thermal theory of laminar flame by Zeldovich – Frank-Kamenetskii [Zeldovich, 1951, Zeldovich et al., 1975, Frank-Kamenetskii, 2015] the pressure-temperature dependence of laminar flame velocity can be expressed as follows:

$$Su(T,p) = Su_0 \left({}^{T}/_{T_0}\right)^{\alpha} \left({}^{p}/_{p_0}\right)^{\beta} \qquad (11)$$

where Su_0 is the laminar flame speed at standard temperature T_0 and pressure p_0; α and β are empirical exponents. Since the laminar flame propagation is controlled by the diffusion of species between reactants and reaction zone, the temperature exponent α is about 1.5, the same as for the ratio of diffusion or thermo-diffusion coefficients $D(T)/D(To)=(T/To)^{3/2}$. Empirical data on α and β exponents at elevated pressures and temperatures are given in Malet, 2005. The data processing of experimental data for cryogenic temperatures by Bavoil (1997) gives the parameters of Eq. (11) in Table 4. As follows from Figure 5, the correlation Eq. (11) is valid in a wide range, including cryogenic temperatures.

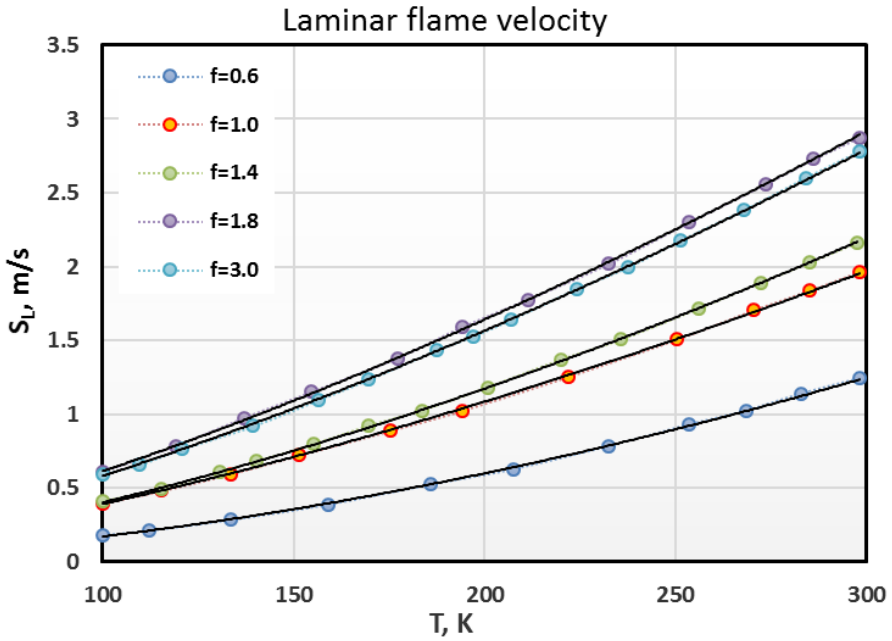

Figure 5. Laminar flame velocity as function of temperature for different hydrogen-air compositions by Bavoil (1997).

Table 4 Laminar flame velocity as function of temperature (Bavoil, 1997))

Equivalence ratio	Laminar flame velocity, Suo, m/s	Temperature exponent α
f=0.6	1.29	1.95
f=1	1.95	1.46
f=1.4	3.06	1.53
f=1.8	3.32	1.4
f=3	2.1	1.55

The laminar flame velocity at different initial conditions can also be directly calculated using the Cantera code with detailed chemistry (Lutz scheme in this particular case). Figure 6 demonstrates the behaviour of laminar flame velocity at low temperatures. The capability of the code was limited by 200K. Then, the dependence was extrapolated to 80K. Figure 6 shows an over-prediction of theoretical calculations compared to experimental data: *Su* = 0.50 m/s against 0.4 m/s (100K). Extrapolation calculations to 80K gives the value *Su* = 0.36 m/s. Since the comparison of experimental and calculated data at ambient temperature 293 gives the same trend *Su* = 2.57 m/s (Cantera) and *Su* = 1.95 m/s (experiments), then the accuracy of calculations is acceptable for further analysis.

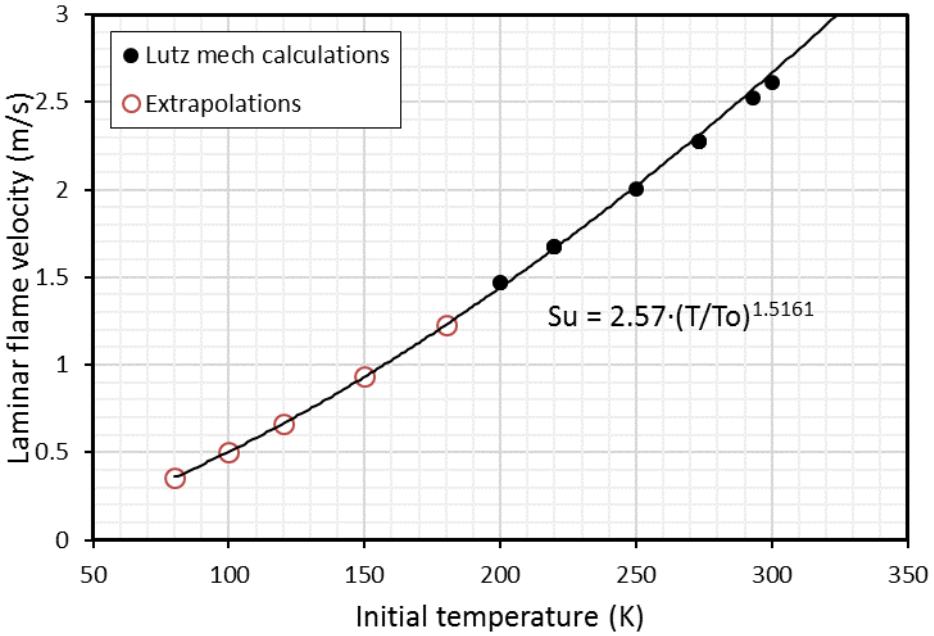

Figure 6. Calculated laminar flame velocity as function of temperature for stoichiometric hydrogen-air mixture (Cantera [Goodwin, 2009] with Lutz mechanism [Lutz, 1988]).

For practical application, we use so-called visible flame speed as a product of laminar flame speed *Su* times expansion ratio σ. As Figure 7 shows, reduced chemical reactivity at cryogenic temperatures will be compensated by higher density and, in turn, by the higher expansion ratio of the gas at low temperatures. It leads that the visible flame velocity 11.7 m/s at T = 80K is only two times lower than that of 25.7 m/s at ambient conditions.

Existing experimental data laminar flame velocity at cryogenic temperatures and its good agreement with theoretical predictions we can use that data for the analysis of flame propagation regimes at reduced and cryogenic temperatures in the current project.

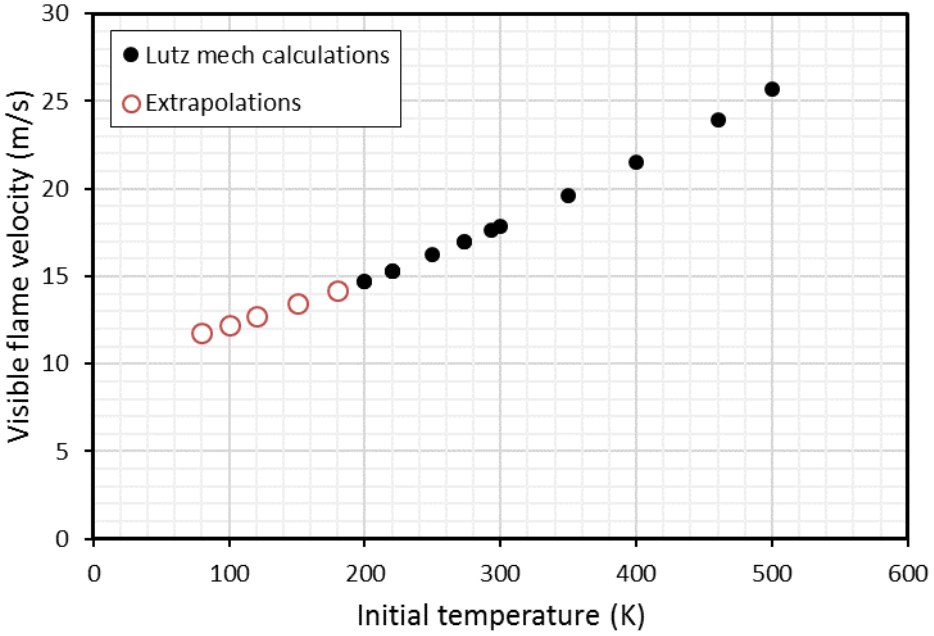

Figure 7. Calculated visible flame velocity as function of temperature for stoichiometric hydrogen-air mixture (Cantera [Goodwin, 2009] with Lutz mechanism [Lutz, 1988]).

3.4. Maximum combustion pressure

Usually, the maximum combustion pressure is associated with adiabatic isochoric combustion pressure P_{ICC}, which can be easily calculated using thermodynamic tables for the equilibrium state of reacting components at constant volume conditions. adiabatic isochoric combustion pressure can be as a measure of the strength of hydrogen-air explosion under conditions of constant volume.

The pressure generated by adiabatic isochoric combustion can be calculated using the EXPLPRESS freeware. This explosion pressure is higher when the initial temperature decreases. For instance, for H_2/air stoichiometric mixture at atmospheric pressure, P_{AICC} equals to 8 bar at 300K increases to 12 and 23.5 bar respectively for 200 and 100 K.

The STANJAN code (W C Reynolds, 1981) and Cantera code [Goodwin, 2009] based on NASA thermodynamic data base are also able to calculate the PICC pressure even to 78K in an assumption of the ideal gas. It gives the same value of 23.49 bar at 100K and 30.08 bar at 78K corresponding to liquid nitrogen temperature. This means that hydrogen explosion at liquid nitrogen temperature will be 3.75 times stronger than at ambient temperature for the same volume of the mixture.

3.5. Maximum combustion temperature

Thermodynamic calculations by STANJAN code demonstrated very weak influence of initial temperature on adiabatic combustion temperature. For instance, a changing of initial temperature from 300 K to 78 K (four times) the adiabatic combustion temperature varies less than about 5%, from 2383 K to 2263 K, respectively.

We suppose that high level of confidence of the theoretical calculations of such thermodynamic characteristics of hydrogen combustion as maximum combustion pressure P_{ICC} and adiabatic combustion pressure Tb at cryogenic temperatures will be sufficient for

direct use of calculated values for the analysis and to normalize real measured combustion characteristics.

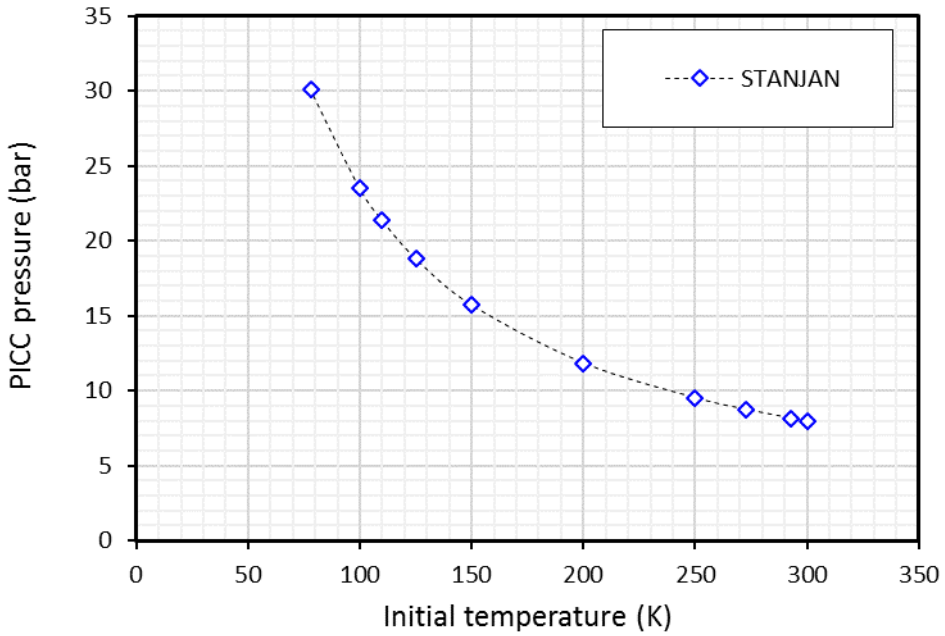

Figure 8. Calculated visible flame velocity as function of temperature for stoichiometric hydrogen-air mixture (STANJAN code, Reynolds, 1981)).

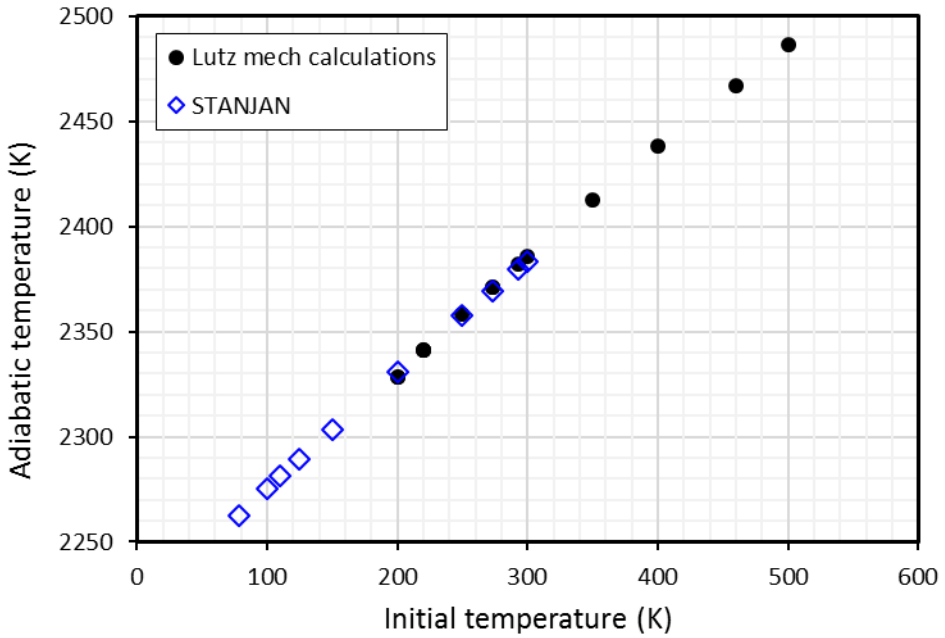

Figure 9. Calculated visible flame velocity as function of temperature for stoichiometric hydrogen-air mixture (Cantera [Goodwin, 2009] with Lutz mechanism [Lutz, 1988]).

3.6. Expansion ratio

The expansion ratio is the ratio of the density of the fresh gases by the density of the burnt gases. This is an important parameter for explosion modeling because it represents the piston effect of the flame due to the thermal expansion of combustion products. This may result in the formation of turbulent flow and advancing shock waves in front of the flame.

Since the visible flame velocity S_f and flow velocity U_f ahead the flame are proportional to the expansion ratio, the expansion ratio is of great importance for combustion processes and flame acceleration and DDT:

$$S_f = \sigma \cdot S_U \; ; \tag{12}$$

$$U_f = (\sigma - 1) \cdot S_U \; , \tag{13}$$

This means that the expansion ratio may also increase roughly in four times assuming a real gas equation of state. As shown in Bavoil (1997) paper, the expansion ratio increases for low temperature. For a stoichiometric mixture at atmospheric pressure, the expansion ratio is equal to 7 at 300K and increases to 20 at 100 K. The same value of expansion ratio σ = 19.53 for the stoichiometric hydrogen-air mixture at 1 bar and 100K was calculated by using the STANJAN code (Figure 10). At 78K the STANJAN code gives a value σ = 24.88.

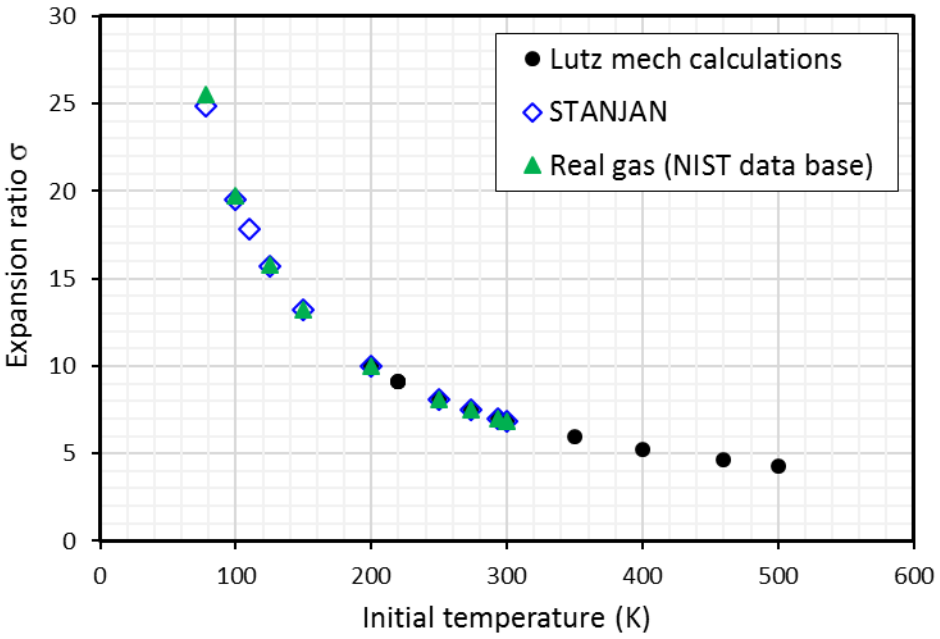

Figure 10. Calculated expansionratio as function of temperature for stoichiometric hydrogen-air mixture (Cantera [Goodwin, 2009] with Lutz mechanism [Lutz, 1988]).

Taking into account the real gas state (according to the NIST data base) at lower initial temperatures the expansion ratio will be not so much changing in comparison with the ideal gas state: σ = 19.73 (T = 100K); σ = 25.53 (T = 78K).

3.7. Concluding remarks

- The proper temperature domain for flammable hydrogen –air mixtures at cryogenic temperatures is defined.
- Since such fundamental properties as expansion ratio, laminar flame velocity and flammability limits will be used for further analysis of flame acceleration and DDT criteria, theoretical evaluations and experimental data extrapolations of such properties at cryogenic temperatures should experimentally be validated.

3.8. References

Baker, N.R., W.D. Van Vorst, Mixture properties for hydrogen supplementation of natural gas, Proc. 2nd World Hydrogen Energy Conf., Zürich/Switzerland, Vol. 3 (1978), pp. 1373-1400

Bavoil Eric (1997), Etude expérimentale de l'influence de la diminution de la température initiale (jusqu'à 100K) sur les déflagrations des mélanges H2-air. 1997-10-15, CNRS, Poitiers, France

DeSoete .G.G. Overall kinetics of nitric oxide formation in flames. La Revista dei Combustibili. 29:166 (1975)

Frank-Kamenetskii, D. A. Diffusion and heat exchange in chemical kinetics. Princeton University Press, 2015.

Gan Cui, Zili Li, Chao Yang, Zhen Zhou and Jianle Li Experimental Study of Minimum Ignition Energy of Methane–Air Mixtures at Low Temperatures and Elevated Pressures, Energy Fuels, 2016, 30 (8), pp 6738–6744

Gasse A. Experimentelle Bestimmung und Simulation von Explosiongrenzen, untersucht an wasserstoffhaltigen Brenngasgemischen. Dissertation Universität-Gesamthochschule Paderborn, Reihe Verfahrenstechnik, Shaker, Aachen (1992)

Goodwin, D., "Cantera: An object-oriented software toolkit for chemical kinetics, thermodynamics, and transport processes", Caltech, Pasadena, 2009. [Online]. Available: http://code.google.com/p/cantera

High, Richard W. Some liquid oxygen / liquid hydrogen explosive effects in controlled failure mode tests NASA report 1969

Hubert Yves Rico Etudes théorique et expérimentale de la détonation des mélanges d'hydrogène liquide et d'oxygène solide à 20 K Thèse de doctorat de l'Université de Paris 1970.

Hustad J.E., Sonju O.K. Experimental studies of lower flammability limits of gases and mixtures of gases at elevated temperatures. Combust. Flame 71:283 (1988)

International Electrotechnical Commission, Electrical apparatus for explosive gas atmospheres - Part 20: Data for flammable gases and vapours, relating to the use of electrical apparatus, Standard IEC 60079-20:2000

Karim G.A., Wierzba I., Boon S. The lean flammability limits in air of methane, hydrogen and carbon monoxide at low temperatures. Cryogenics, 24(6), 1984, pp.305–308

Kumar R.K. Flammability limits of hydrogen-oxygen-diluent mixtures. AECL-8890. Journal of Fire Sciences, 3:245-262 (1985)

Kuznetsov M., Czerniak M., Grune J., Jordan T., Effect of temperature on laminar flame velocity for hydrogen-air mixtures at reduced pressures. Proc. of the 5th International Conference on Hydrogen Safety, ICHS 2013 September 9-11, 2013 - Brussels – Belgium, paper 231, p. 1-12

Kuznetsov, M., R. Redlinger, Flammability limits of hydrogen-air and hydrogen-oxygen mixtures at elevated temperatures. 2nd quarter report, IceFuel Project, 2008

Lewis, B., G. von Elbe: Combustion, Flames and Explosions of Gases, Academic Press, Orlando, San Diego, New York, Austin, Boston, London, Sydney, Tokyo, Toronto 1987. 739 p.

Lutz, A.E., "A Numerical Study of Thermal Ignition", Sandia Report SAND88-8228 (1988).

Malet, F., “Etude experimentale et numerique de la propagation de flammes premelangees turbulents dans une atmosphere pauvre en hydrogene et humide”; PhD Thesis de l’Universite d’Orleans (2005)

Manion, J. A., R. E. Huie, R. D. Levin, D. R. Burgess Jr., V. L. Orkin, W. Tsang, W. S. McGivern, J. W. Hudgens, V. D. Knyazev, D. B. Atkinson, E. Chai, A. M. Tereza, C.-Y. Lin, T. C. Allison, W. G. Mallard, F. Westley, J. T. Herron, R. F. Hampson, and D. H. Frizzell, NIST Chemical Kinetics Database, NIST Standard Reference Database 17, Version 7.0 (Web Version), Release 1.6.8, Data version 2015.09, National Institute of Standards and Technology, Gaithersburg, Maryland, 20899-8320. Web address: http://kinetics.nist.gov/

Martín-Valdepeñas, J M, M A Jiménez, Exploring MIE as a Safety Indicator Parameter in Practical Applications, Universidad Politécnica De Madrid Escuela Técnica Superior De Ingenieros Industriales, Cátedra De Tecnología Nuclear, EU-Fifth Framework Programme (1998-2003), Contract EVG1-CT-2001-00042, EXPRO - Experimental and Numerical Study of Reactive Flows with Relevance to Industrial Safety for Explosion Protection, CTN-09/03, November 2003

National Aeronautics and Space Administration Report, Safety Standard for Hydrogen and Hydrogen Systems, Report NSS 1740.16, 1997, p. A-16.

Omar, M.H.; Z. Dokoupil Solubility of nitrogen and oxygen in liquid hydrogen at temperatures between 27 and 33°K, Physica, Volume 28 issue 5 1962

Reynolds, W C, STANJAN: interactive computer programs for chemical equilibrium analysis. Stanford University. Thermosciences Division. January 1981.

Wierzba K. Harris G.A. Karim Effect of low temperature on the rich flammability limits in air of hydrogen and some fuel mixtures containing hydrogen International Journal of Hydrogen Energy Volume 17, Issue 2, February 1992, Pages 149-152

Zabetakis M.G. Flammability characteristics of combustible gases and vapors, BuMines Bulletin 627, p. 121 (1965)

Zeldovich, Y B, Theory of flame propagation, Washington, NACA TM 1282, 1951, Translated Zhurnal Fizicheskoi Khimii (USSR). Vol. 22, pp.27-49, 1948.

Zeldovich, Y.B., Barenblatt, G.I., Librovich, V.B., and Makhviladze, G.M. Mathematical theory of combustion and explosions. United States: N. p., 1985.

4. Cryogenic hydrogen combustion. A theory, experiments, accidents and numerical simulations (KIT)

The objective is to evaluate critical conditions for flame acceleration and detonation transition for hydrogen-air mixtures at cryogenic temperatures, possibly in presence of condensed oxygen and nitrogen. The data are required for safety analysis to evaluate the strongest possible combustion pressure and safety distances for LH2 explosions.

4.1. Cryogenic hydrogen jet-fire (KIT, UU, PS)

In this particular chapter, the main characteristics of cryogenic hydrogen jet fire are analyzed as following: flame length, heat radiation, maximum combustion pressure and damage diagrams for safety distance evaluations. An effect of jet geometry, nozzle diameter, initial bulk pressure and temperature will be analyzed.

4.1.1. Dimensionless flame length correlations (UU)

Sandia National Laboratories (SNL) conducted experiments on cryogenic hydrogen jet fires with release temperature 37-295 K and pressures up to 6 bar abs (Panda & Hecht, 2017). They observed that the flame length correlates well with the square root of the Reynolds number. The dimensionless correlation for hydrogen jet flames developed at Ulster includes treatment of non-premixed flames from expanded and under-expanded releases through the Mach and Froude numbers in addition to Reynolds number (Molkov & Saffers, 2013). The correlation was validated against jet fires with pressure in the range 10-900 bar and temperature in the range 187-300 K. UU analysed the performance of the dimensionless correlation when applied to model 30 tests on vertical cryogenic hydrogen jet fires conducted at SNL (Cirrone et al., 2019). Release temperature and pressure were included in the ranges 46-295 K and 2-6 bar abs respectively. Ulster's under-expanded jet theory was applied to calculate parameters at the real nozzle exit (Molkov et al., 2009). The deviation of the calculated mass flow rate from experiments was contained within ±10%. The experimental flame length was given as an average of the images of the visible and infrared (IR) cameras. Correlation by Schefer et al. (2006), $L_{vis} = 0.88\, L_{IR}$, was used to retrieve the visible flame length in SNL tests and report the results in Figure 11.

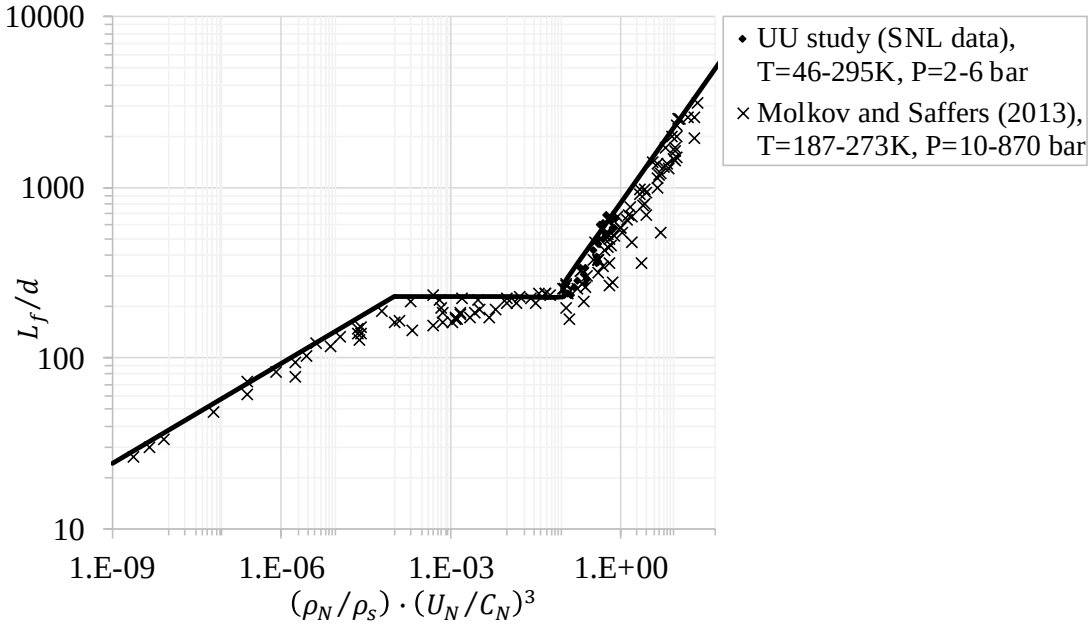

Figure 11. The dimensionless correlation for hydrogen jet flames against experiments.

All tests are located in the momentum dominated under-expanded jet region. It is showed that the flame correlation represents conservatively SNL cryogenic jet fires. Three tests with release pressure equal to 2 bar abs present an exception out of the set of 30 tests, showing an underestimation of the flame length up to 14%. This deviation may be due to the experimental determination of the flame length as the distance from the nozzle where the intensity drops to 10% of the maximum recorded for the flame image. Overall, the

deviation of calculated flame length from experimental measurements is mostly within acceptable accuracy for engineering correlations, 20%, similarly to releases from storage at atmospheric temperatures. It is concluded that the use of the dimensionless flame correlation can be expanded to cryogenic releases with pressure up to 6 bar abs.

The temperature at the release was found to greatly affect the resulting flame length. Considering as an example a release pressure of 2 bar abs and nozzle diameter 1.25 mm, the decrease of temperature from 185 K to 46 K leads to an increase of calculated flame length from 0.40 m to 0.77 m. As a consequence, the minimum distance to not be harmed by the jet fires should increase from 1.4 m to 2.7 m. Calculation of "no harm" distance follows the study in (Molkov & Saffers, 2013), that related the jet fire flame length and temperature distribution along the axis. It was found that the temperature of 70 ºC, which corresponds to a "no harm" criteria for any exposure duration, is achieved at $x = 3.5L_f$.

Panda and Hecht (2016) studied cryogenic hydrogen ignited free releases. They compared own data on jet fire length with known literature (Figure 12) and showed that the correlation Eq. (14) established for gaseous hydrogen releases could be used for cryogenic hydrogen releases as well:

$$\frac{L_f}{D} = 0.86\sqrt{\mathrm{Re}} \tag{14}$$

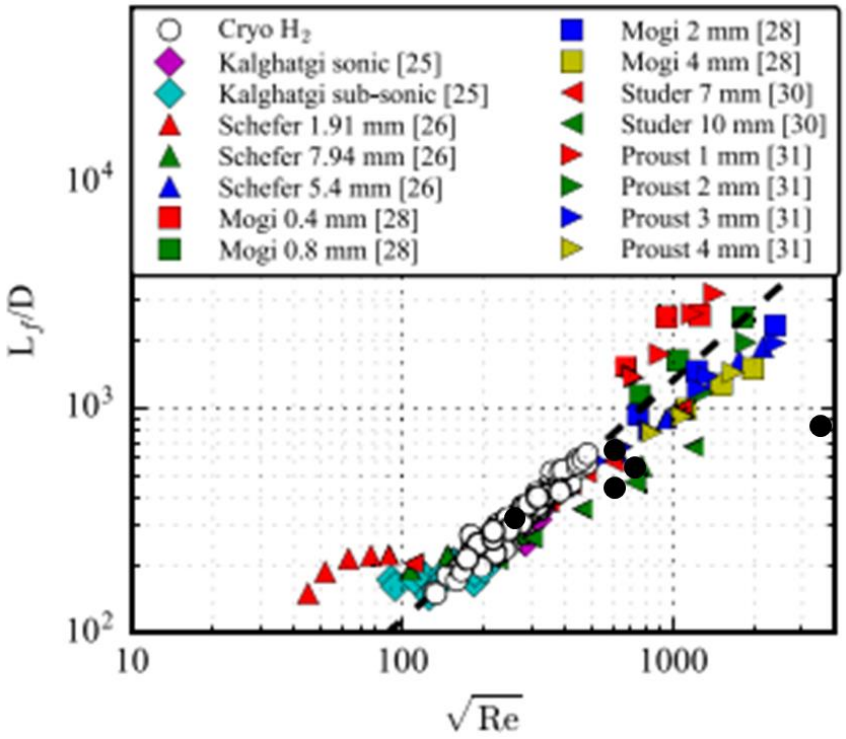

Figure 12. Dimensionless flame length as a function of Reynolds number for the cryogenic hydrogen releases by Panda and Hecht (2016). Black symbols correspond to data (Breitung et al., 2009)

The Reynolds number is calculated on the throat density, viscosity, choked flow velocity, and diameter. Compared to the expression proposed by Molkov and Saffers (2013) ($L_f = f(m.D)^{½}$) for atmospheric temperature hydrogen releases, this expression allows to take into consideration the variations in viscosity extends the correlation for cryogenic hydrogen

releases. Experimental data by Panda and Hecht (2016) also give a proportionality of flame length Lf against mass flow rate at different temperatures. The proportionality coefficient is higher for cryogenic temperatures.

The visible flame length of turbulent diffusion flames has been extensively investigated in Panda and Hecht (2016) and Sivathann and Gore (1993), Houf and Schefer, (2007), and Breitung et al. (2009). They represent a summary plot for the non-dimensional visible flame length L* as a function of Froude number (Figure 13, Figure 14), where

$$L^* = L_{vis}\frac{f_s}{d}\left(\frac{\rho_\infty}{\rho_o}\right)^{1/2} \tag{15}$$

L_{vis} is the visible flame length; f_s is the mass fraction of hydrogen in a stoichiometric H_2-air mixture (29.6 vol. %); d is the nozzle diameter; ρ_o is the density in a pressurized reservoir; ρ_∞ is the density of ambient air. Low Froude numbers refer to slow buoyant plumes. The most dangerous jet fires have Fr-numbers larger than 5, for which L* = 23 can be assumed with good accuracy, so that the visible flame length can be expressed as a simple function of the nozzle diameter d and the hydrogen reservoir density ρ_o:

$$L_f = 23\frac{d}{f_s}\left(\frac{\rho_0}{\rho_\infty}\right)^{1/2}, \tag{16}$$

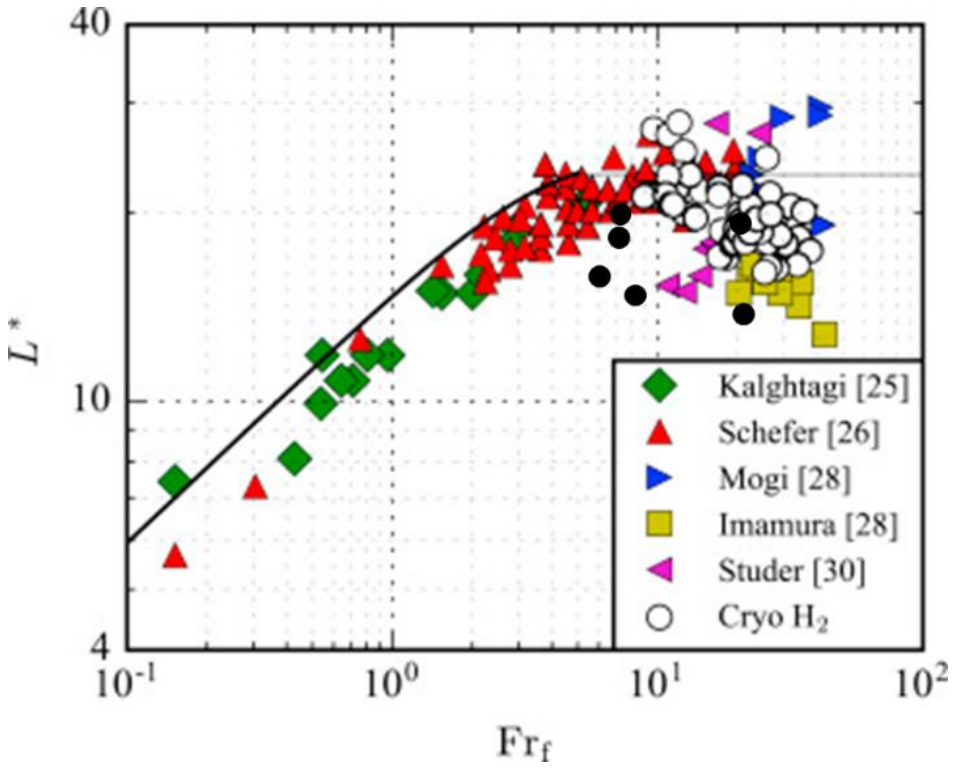

Figure 13. Dimensionless flame length as a function of Reynolds number for the cryogenic hydrogen releases by Panda and Hecht (2016). Black symbols correspond to data (Breitung et al., 2009)

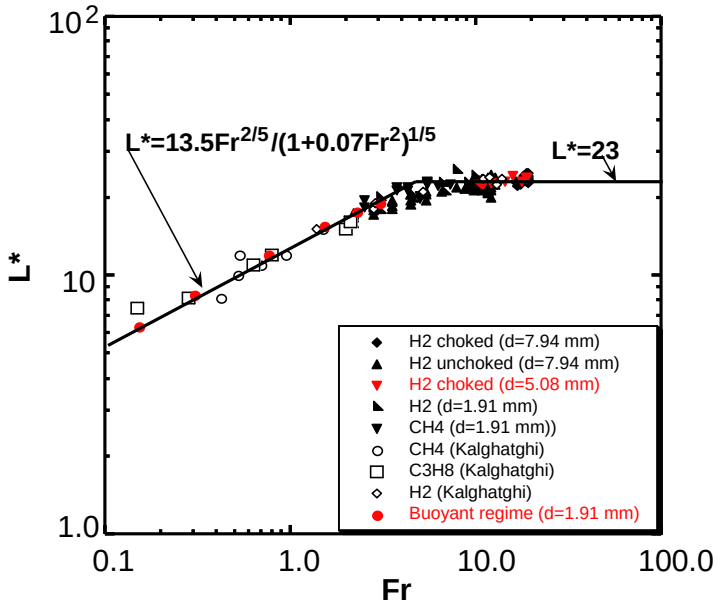

Figure 14. Non-dimensional visible flame length as a function of Froude number for the cryogenic hydrogen releases: black symbols (Sivathann and Gore, 1993) red symbols (Houf and Schefer, 2007); open symbols (hydrocarbons).

4.1.2. Heat radiation and radiative fraction

Heat flux from hydrogen jet fire is one of the major properties to be used for safety distance evaluations. Radiative emission of hydrogen jet fire behaves as grey body radiation and depends on the optical thickness of the radiative zone. Taking into account the hydrogen jet fire structure and different diameters of jet fire along the axis, it should be an axial and radial distribution of heat flux radiation out of the flame surface. Independent of the gas nature the maximum heat flux occurs at the axial position x/Lf = 0.6 (see Figure 15). The same results were obtained for cryogenic hydrogen releases as a function of heat flux versus normalized axial position x/Lf (see Figure 16). The temperature changed up to 48K in this work.

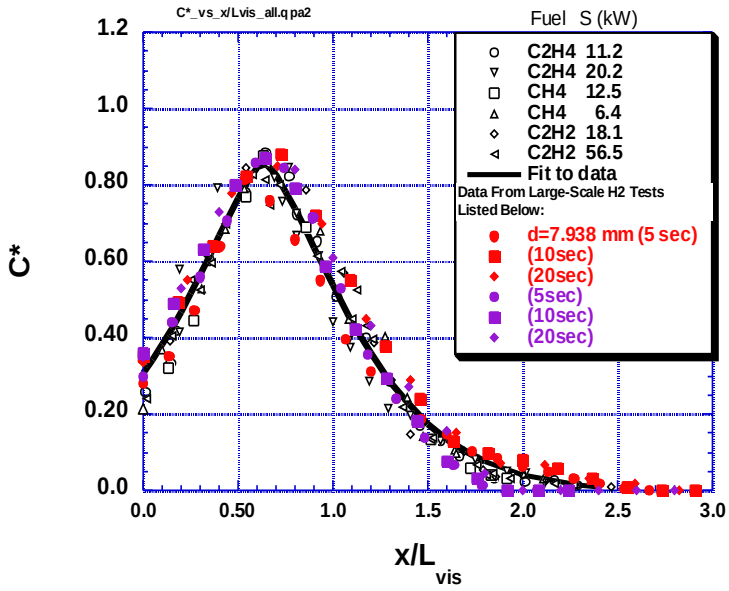

Figure 15. Profiles of normalized radiative heat flux along the centerline of a turbulent, hydrogen-jet flame. Jet diameter is 7.94 mm. Vertical jet orientation [Schefer et al., 2006].

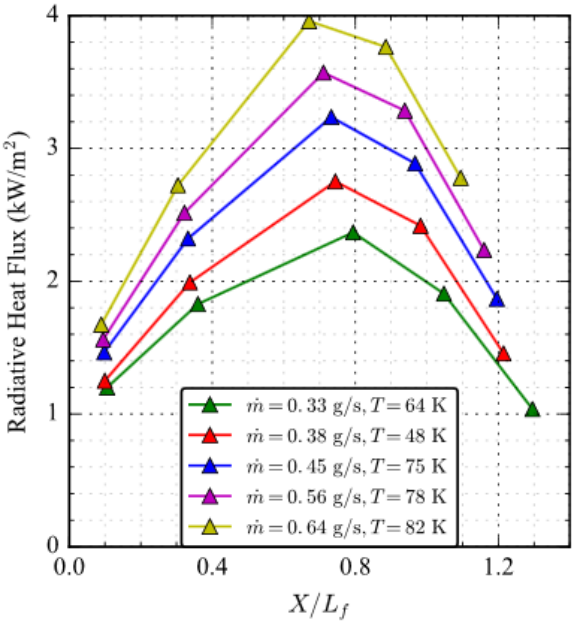

Figure 16. Radiative heat flux along the length of the jet flame, for several cold release conditions. [Panda and Hecht, 2016].

In the framework of the Icefuel project, a series of experiments with cryogenic hydrogen releases at initial pressures from 7 to 35 bars and temperatures from 35 to 80 K was performed (Breitung et al., 2006; Friedrich et al., 2012). Radiative levels of jet flames were measured at different radial and axial positions. The axial sensor locations were changed from 0.25 to 2.25 m from the nozzle level at three fixed radial locations 0.50, 0.75 and 1.25 m from the jet axis.

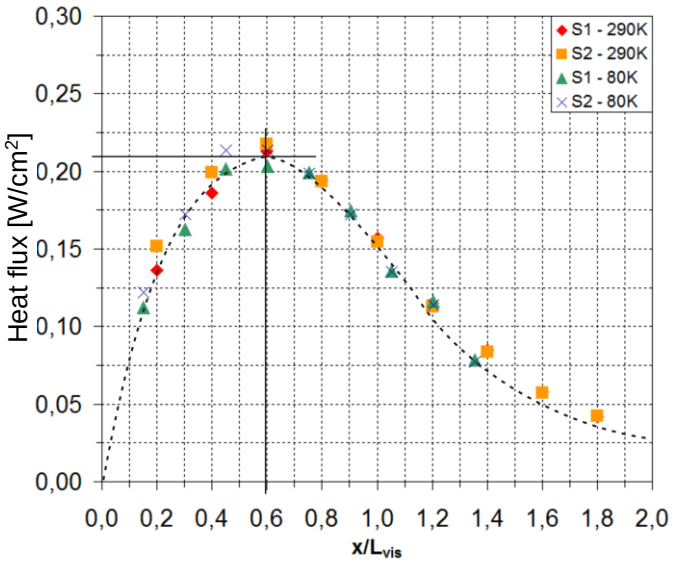

Figure 17. Measured heat fluxes scaled in axial and radial direction with the visible flame length L_{vis} (r/L_{vis} = 0.5) (Breitung et al., 2006).

Figure 17 shows a plot of heat fluxes versus x/L_{vis} for a constant scaled radial distance of r/L_{vis} = 0.5. This scaled radial distance corresponds to absolute radial distances between 0.625 and 1.04 m. Heat flux measurements were made for radial distances of r = 0.5, 0.75, and 1.25 m, so that the heat fluxes at r/L_{vis} = 0.5 can be interpolated from the data shown

in Figure 17. This scaling approach results in a single relation which has its maximum at x/L_{vis} = 0.6. The maximum heat flux in these scaled coordinates is q_{max} = q(x/L_{vis} = 0.6, r/L_{vis} = 0.5) = 0.21 W/cm^2.

The measured maximum heat fluxes from the data similar to Figure 17 but for all the experiments can also be scaled against the radial coordinate r/L_{vis}. The resulting 6×3 = 18 data points are plotted in Figure 18; they all follow closely to the relation

$$q_{max} = 0.74\left(\frac{r}{L_f}\right)^{-1.59} \frac{kW}{m^2} \qquad (17)$$

Of course, it should be a difference of radial heat flux distribution for jet fire geometry and classical spherical geometry of fireball when heat flux decays proportionally to r^{-2}.

Maximum heat flux is the most important characteristic of burned hydrogen jet for conservative hazard evaluation. For x/L_{vis} = 0.5, Eq. 17 reproduces well the maximum heat flux from Figure 18. The correlation of q =q(x/L_{vis}) together with Eq. 17 allows to calculate q(x,r) for a given visible flame length L_{vis}.

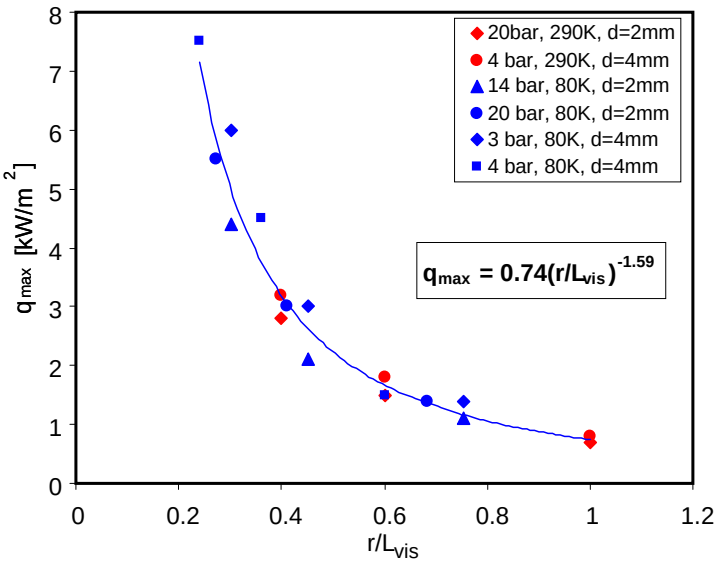

Figure 18. Measured maximum heat fluxes as function of scaled radial distance r/L_{vis} from the jet axis, r= radial distance, L_{vis} = visible flame length (x/L_{vis} = 0.5) (Breitung et al., 2006).

One more useful correlation of heat flux and mass flow rate at cryogenic temperatures is given in Figure 19 (Breitung et al., 2006):

$$q_{r=0.75m}\left[\frac{W}{cm^2}\right] = 0.1275\dot{m}_{H2}\left[\frac{g}{s}\right] \qquad (18)$$

The heat flux calculated by Eq. 18 can be recalculated for any distance assuming a certain geometry (cylinder, spherical). This correlation is quite similar to that as a function of flame length (Eq. 17).

Since hydrogen flame is very transparent and radiates as a grey body, the emissivity of such flame depends on the optical thickness of the flame. The measurement of the local heat flux q(x,r) parallel to the jet axis at a radial distance r = L_{vis} /2, allows to derive the total heat

flux S_{rad} emitted from the flame by integrating q(x,r) over a cylindrical surface with the radius r = L_{vis} /2. When S_{rad} is divided by the chemical heat release rate the fraction of radiant energy X_{rad} can be calculated:

$$X_{rad} = \frac{S_{rad}}{\dot{m}\,\Delta H_c} = \frac{\int_{cyl.} q(x, r = L_{vis}/2)\, dA}{\dot{m}\,\Delta H_c} \qquad (19)$$

where S_{rad} is the total emitted thermal energy of the jet flame; $\dot{m}$ is the release rate of hydrogen = burning rate; ΔH_c = 120 MJ/kg is the heat of hydrogen combustion; q(x,r=L_{vis}/2) is the measured local heat flux at r = L_{vis}/2; dA is the surface element of a cylinder, assumed for jet fire shape.

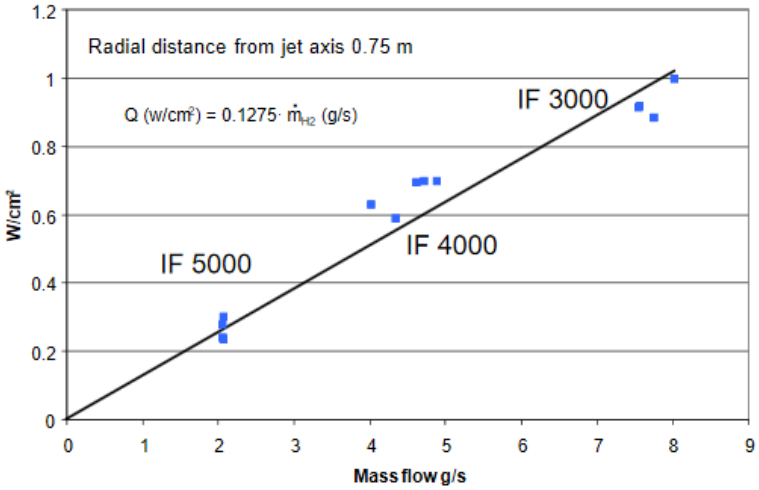

Figure 19. Radiation heat flux correlation as function of mass flow rate (Breitung et al., 2006). Initial temperatures To = 34-65K (IF 3000); To = 38-44K (IF 4000); To = 44K (IF 5000).

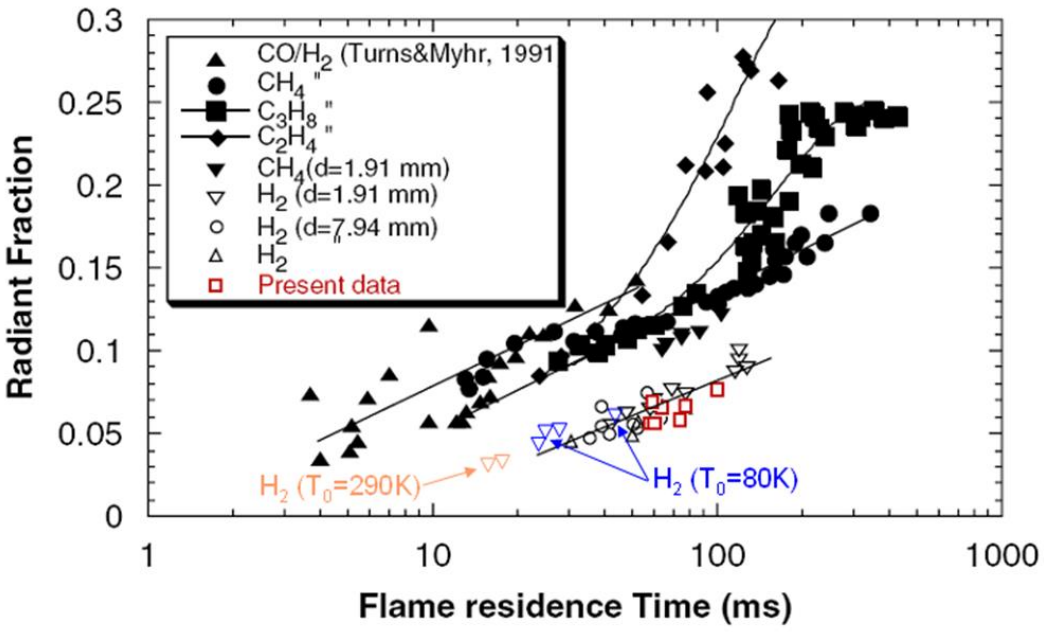

Figure 20. Comparison of radiant fractions obtained in different works: black open points (hydrogen, Schefer et al., 2006); black solid points (hydrocarbons, Turns and Myhr, 1991) red and blue open points (hydrogen at different temperatures, Breitung et al. (2006).

The results obtained by Breitung et al. (2006) for the radiant fraction are compared in Figure 20 to the literature data (Schefer et al., (2006); Turns and Myhr, 1991) in terms of radiant fraction x_{rad} as a function of residence time τ. The flame residence time τ, as defined in Turns and Myhr (1991), is the average time a volume of burned gas needs to pass through the jet flame region. τ is proportional to flame length L_{vis}. It follows Figure 20:

1. Thermal radiation from hydrogen flames is significantly below that of hydrocarbons, where the radiative properties are dominated by continuum radiation from solid soot particles. In hydrogen jet flames gas band radiation from steam is the dominant emitting mechanism, resulting in much less heat release. This is an important safety advantage of GH_2-flames compared to hydrocarbon jet flames.

2. According to Schefer at al. (2007) and Turns and Myhr (1991), the radiant fraction increases with the residence time and visible flame length ($\tau \sim L_{vis}$).

3. According to Breitung et al. (2006) the radiant fraction of hydrogen jet fire is increasing from 3 to 8% with initial temperature decrease from 290 to 34K.

Another series of hydrogen jet fire radiation measurements were performed by Panda and Hecht (2016) at cryogenic and normal initial temperatures (Figure 21). The paper shows the same trend for radiant fraction versus nozzle temperature. The radiant fraction increases from 1.5 to 5% with temperature decrease from ambient (300K) to cryogenic temperature (60K). A correlation based on power-law was proposed to predict the radiative fraction as a function of global flame residence time

$$\chi_r = 9.45 \times 10^{-9} \left[a_p \tau_G T_f^4 \right]^{0.47}. \quad (20)$$

where τ_G is the residence time; Tf is the adiabatic flame temperature; $a_p = 0.23$ is the Planck-mean absorption coefficients for different flames reported by Molina et al. (2007).

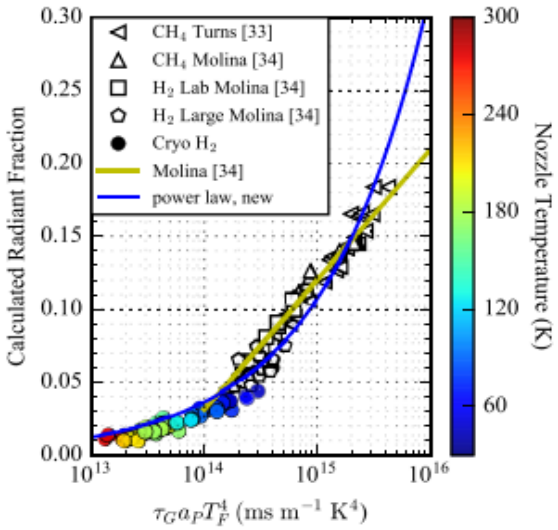

Figure 21. Radiant fractions for the cryogenic hydrogen jet flames (Panda and Hecht, 2016).

4.1.3. Damage diagram

The aforementioned analysis of hydrogen jet fire dimensions and its heat radiation allows evaluating the integral heat flux under jet fire effect on surrounding structures and humans in the vicinity of the hydrogen jet release for potential risk assessment and safety distances

evaluations. The total heat flux is an integral of local specific heat flux over the jet fire surface. Then, we have to know the axial heat flux distribution along with the jet fire (see Figure 15, Figure 16, Figure 17), radial distribution (Figure 18) and the shape of the jet fire surface. Of course, for each particular case, an integral heat flux can be numerically integrated with proper models of high-pressure hydrogen release, its distribution, combustion model and radiation of combustion products. To simplify the problem a cylinder shape of the jet fire with characteristic length L = L_f and a side surface of S = 0.17 L_f^2 in average was assumed (Breitung et al., 2006). The cylinder shape of hydrogen jet fire could be based on Figure 22 (Schefer et al., 2006). The ratio of visible flame width to visible flame length was found to be 0.17 ± 0.02 in many experiments (Schefer et al., 2006; Turns and Myhr, 1991) and the maximum dimension is roughly located in the middle position of the jet. The effect of heat radiation depends on the jet fire orientation with respect to the object. It can be horizontal, vertical and a side or an axial view position. For the axial view position, the radiative area was assumed as S = 0.02 L_f^2 (Figure 23).

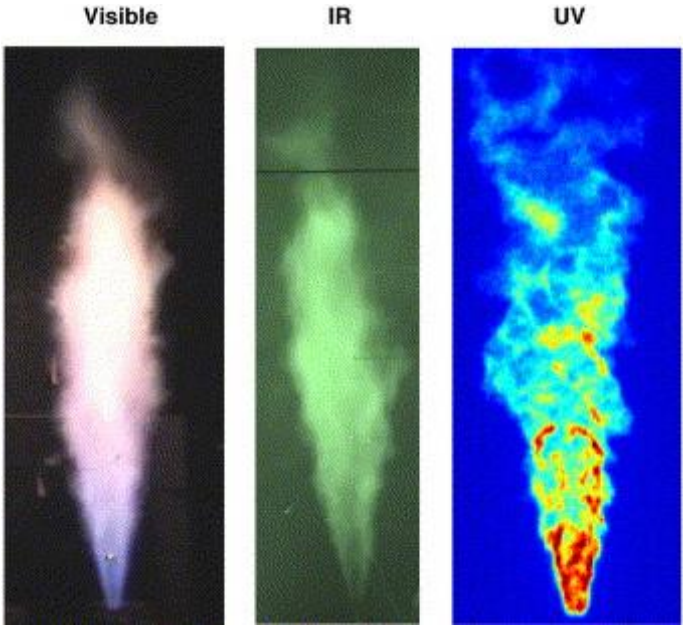

Figure 22. Visible, IR and UV images of turbulent, hydrogen-jet flame (Schefer et al., 2006).

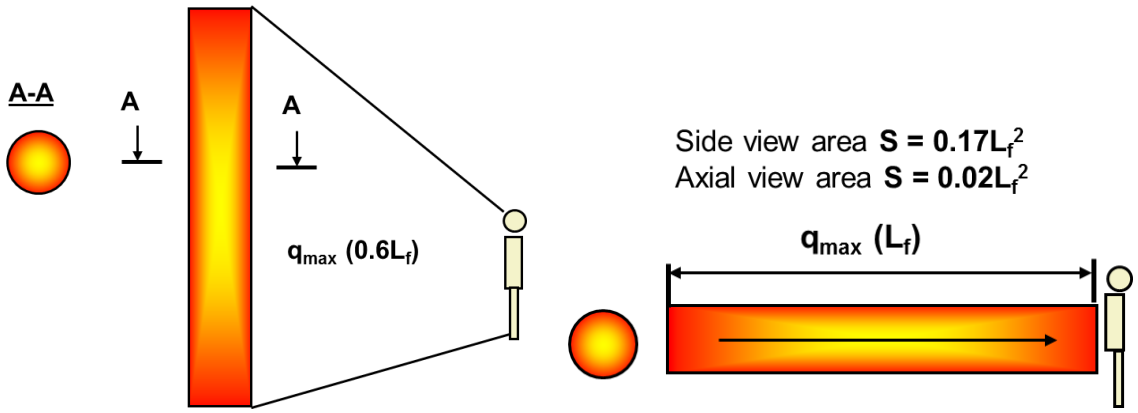

Figure 23. Geometry of hydrogen jet fire and exposing object location (Breitung et al., 2006): left – side position; right – axial position of exposing object.

As proposed in Breitung et al. (2006), for most of the realistic accident cases with Fr > 5, a correlation (Eq. 16) can be used for visible jet fire dimension L_f

$$L_f = 23 \frac{d}{f_s} \left(\frac{\rho_0}{\rho_\infty}\right)^{1/2} ,$$

where f_s is the mass fraction of hydrogen in stoichiometric H2-air mixture; d is the nozzle diameter; ρ_0 is the density in the pressurized reservoir; ρ_∞ is the density of ambient air. Eq. 16 allows to scale the maximum heat fluxes to any required nozzle diameters and hydrogen reservoir densities connected to the pressure and temperature of pressurized volume. The extrapolation of q_{max} assumes conservatively that the exposed object surface is located near the axial position $x/ L_f = 0.6$, or roughly in the middle of the axial jet flame at a certain radial distance r. Then, Eq. 17 can be used to calculate the maximum heat flux at radial position r :

$$q_{max} = 0.74 \left(\frac{r}{L_f}\right)^{-1.59} \frac{kW}{m^2}$$

Based on this approach Figure 24 shows the calculated radial safety distances L_s at which the skin pain limit of about 50 kJ/m^2, (Mudan, 1984) which is close to 1st degree of skin damage (Stoll and Chianta, 1968; Sullivan and Jagger 2004) would be reached after 10 seconds of thermal exposure. This distance may be considered as the safe distance because usually 10 s should be a sufficient time to take protective measures against the heat flux. The safety distances in Figure 24 are proportional to the nozzle diameter and the square root of the hydrogen density in the reservoir. For a given pressure the safety distance decreases with increasing temperature, due to the density reduction. It also shows that cryogenic temperatures will lead to enlarged safety distances at the same bulk pressure.

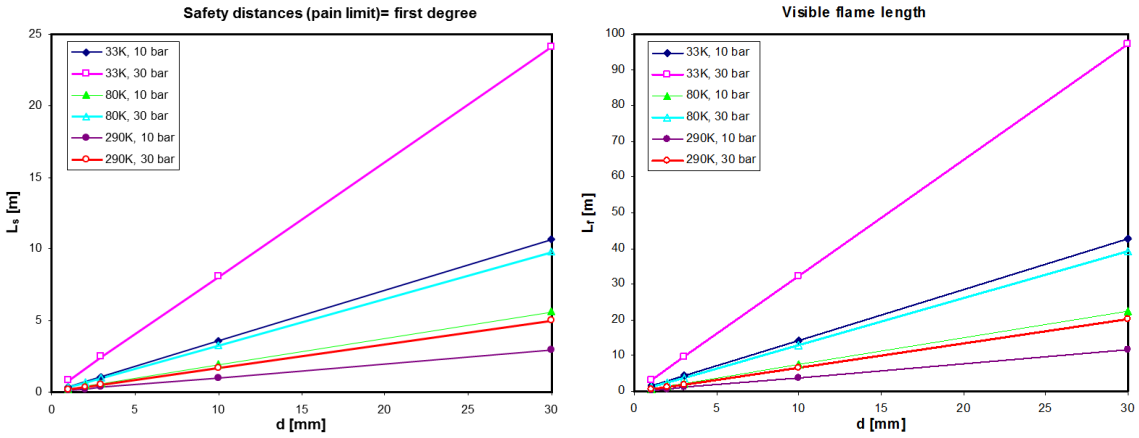

Figure 24. Estimated radial (left) and axial (right) safety distances for reaching the skin pain limit within 10 seconds (Breitung et al., 2006). The visible flame length L_f is used as safety distance for axial position. The effects of leak diameter and hydrogen reservoir conditions are shown.

For the axial position, the visible flame length can be considered as an axial safety distance for flammable materials or humans and structures. The safety distances equal to flame length L_{vis} based on Eq. 16 are presented in Figure 24, right for different break diameters d and hydrogen reservoir conditions.

Figure 25 presents another view on thermal hazards by considering the exposure time necessary to reach a given skin damage. Skin damage depends primarily on the absorbed radiative energy and weakly on radiative power. Figure 25 summarizes the energies needed for the different degrees of skin damage (Stoll and Chianta, 1968; Sullivan and Jagger 2004). Five lines are shown for scaled radial distances of r/L_{vis} = 0.1 -1.0 from jet fire axis.

Their slopes correspond to the maximum heat fluxes from Eq. (17), e.g. 9.56 kW/m^2 for r/L_{vis} = 0.2. A cross-section of r/L_{vis} – line with a certain damage degree corresponds to the safety distance to reach a certain damage degree in the corresponding exposure time exceeds the critical value corresponding to the cross-section point. The value r/L_{vis} = 0.1 represents the lower limit of the present model because the ratio of visible flame width to visible flame length was found to be 0.17 ± 0.02 in many experiments (Schefer et al., 2006; Turns and Myhr, 1991). The radial distance of r/L_{vis} = 0.1 is therefore close to the visible flame surface.

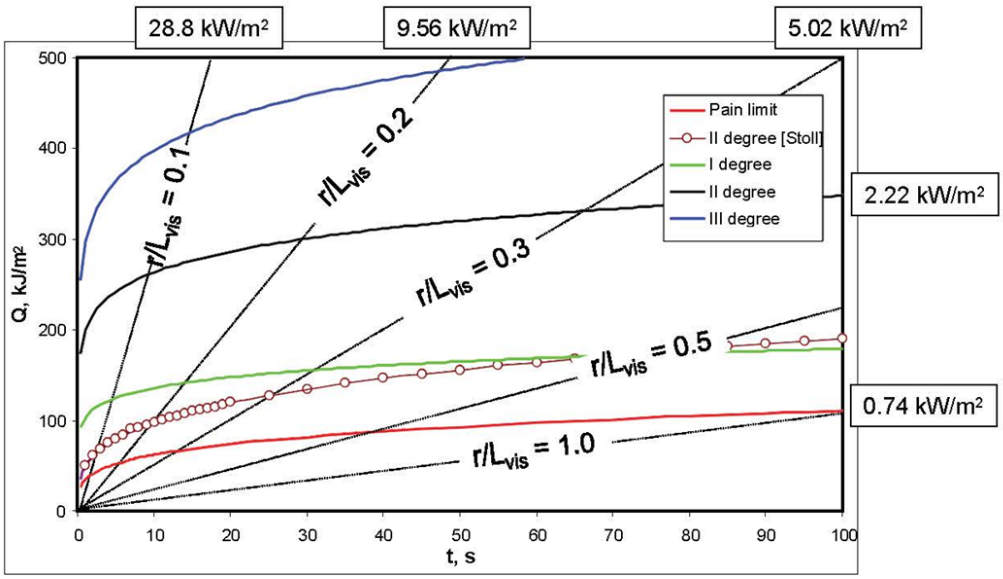

Figure 25. Maximum exposure times for different degrees of skin damage from thermal radiation of turbulent hydrogen gas jet flames.

Using the visible flame lengths from Figure 24, right, the maximum exposure times for different skin damages can be estimated from Figure 25. For instance, for an 80 K/30 bar reservoir with a 10 mm leak the safety distance L_{vis} is about 12 m. At an absolute distance of r = 3.6 m (r/L_{vis} = 0.3) the pain limit would be reached after 10 s, the first, second and third degree of skin damage after about 20 s, 50 s, and 80 s, respectively. The most sensitive surface for thermal radiation is the eye.

The only damage diagrams due to thermal radiation of hydrogen jet fire are analyzed. The effect of combustion pressure and blast wave under high pressure hydrogen release is not presented in this chapter due to the lack of experimental data.

4.1.4. Concluding remarks

This section can be summarized as follows:

- Based on existing experimental data the visible flame length L_{vis} for a cryogenic hydrogen jet fire can be evaluated. The data should be extended for horizontal jet fire as well. The shape and characteristic dimensions of cryogenic jet fire should be investigated more precisely.
- There is a lack of heat flux measurement for cryogenic jet fire. Thermal radiation from horizontal stationary high-momentum hydrogen jet flames at cryogenic temperatures should be measured using thermo-video camera. Time dependence of heat flux for unstationary jet fire should also be investigated. CFD models for numerical simulation of jet fire radiation should be developed.

- Spatial distribution of heat radiation from jet fire should be investigated.
- An ignition envelope and flame flush back limit for cryogenic hydrogen jet should be investigated.
- Transient regimes of cryogenic jet fire should be investigated with respect to measure heat radiation and maximum combustion pressure at the initial moment of jet fire development, just after ignition.
- A more precise (not so conservative) procedure for damage diagrams due to heat radiation and blast wave under hydrogen jet ignition should be developed.

4.1.5. References

Breitung, W., G. Stern, A. Veser, A. Friedrich, M. Kutznetsov, G. Fast, B. Oechsler, N. Kotchourko, J.R. Travis, J. Xiao, M. Schwall, M. Rottenecker (2009), Experimental and theoretical investigations of sonic hydrogen discharge and jet flames from small breaks. Icefuel, Endbericht/Final report #16 SV 2358, KIT/Research Center Karlsruhe, December 2009.

Cirrone, D., Makarov, D. and Molkov, V. (2019), Cryogenic hydrogen jets: flammable envelope size and hazard distances for jet fire, International Conference on Hydrogen Safety, Adelaide, Australia.

Friedrich, A., W. Breitung, G. Stern, A. Veser, M. Kuznetsov, G.Fast, B.Oechsler, N. Kotchourko, T.Jordan, J.R.Travis, J.Xiao, M.Schwall, M.Rottenecker, (2012) Ignition and heat radiation of cryogenic hydrogen jets International Journal of Hydrogen Energy 37(22): 17589-17598

Houf ,W., R. Schefer, (2007), Predicting radiative heat fluxes and flammability envelopes from unintended releases of hydrogen, Int. Journal of Hydrogen Energy, 32(1): 136-151

Molina, A., R. W. Schefer, W. G. Houf, (2007) Radiative fraction and optical thickness in large-scale hydrogen-jet fires, Proceedings of the Combustion Institute, 31(2): 2565-2572

Molkov, V. and Saffers, J. B. (2013), Hydrogen Jet Flames, International Journal of Hydrogen Energy, vol. 38, no. 19, pp. 8141–8158.

Molkov, V., J.-B. Saffers, (2013), Hydrogen jet flames, International Journal of Hydrogen Energy, 38(19): 8141-8158.

Molkov, V., Makarov, D. and Bragin, M. V. (2009), Physics and Modelling of Underexpanded Jets and Hydrogen Dispersion in Atmosphere, Physics of Extreme States of Matter, pp. 146–149.

Mudan KS (1984) Thermal radiation hazards from hydrocarbon pool fires. Prog Energy Combust Sci, 10:59–80

Panda, P. P. and Hecht, E. S. (2017), Ignition and Flame Characteristics of Cryogenic Hydrogen Releases, International Journal of Hydrogen Energy, vol. 42, no. 1, pp. 775–785.

Pratikash, P. Panda, Ethan S. Hecht Ignition and flame characteristics of cryogenic hydrogen releases International Journal of Hydrogen Energy, Volume 42, Issue 1, 5 January 2017, Pages 775-785

Schefer, R.W., W.G. Houf, B. Bourne, J. Colton, (2006) Spatial and radiative properties of an open-flame hydrogen plume, International Journal of Hydrogen Energy, 31(10) : 1332-1340

Sivathann, Y.R., J.P. Gore, Total radiative heat loss in jet flames from single point radiative flux measurements, Combustion and Flame 94 (1993) 265 – 270.

Stoll, A.M., Chianta, M.A., Method and rating system for evaluation of thermal protection, Aerospace Medicine, Vol. 40 (1968) pp. 1232-1238

Sullivan, S. Jagger, S. Human valurability to thermal radiation, Offshore, Harpur Hill, Buxton, Derbyshire, SK179JN, HSL/2004/04

Turns, S.R., F.H. Myhr, Oxides of nitrogen emissions from turbulent jet flames: Part I—Fuel effects and flame radiation, Combustion and Flame 87 (1991), 319-335.

4.2. Flame propagation regimes at cryogenic temperatures (KIT)

Within the flammability limits, three typical combustion regimes can be distinguished for gaseous mixtures. These include slow subsonic deflagrations ($v < c_r$ - flame velocity v is less than the sound speed in reactants c_r), fast supersonic flame ($c_r < v < c_p$ - flame velocity was less than the sound speed in products c_p, but more than the sound speed in reactants), and detonation ($v = D_{CJ}$, Chapman-Jouguet velocity). All possible regimes are shown schematically in Figure 26 for hydrogen-air mixtures at initial pressure 1 bar.

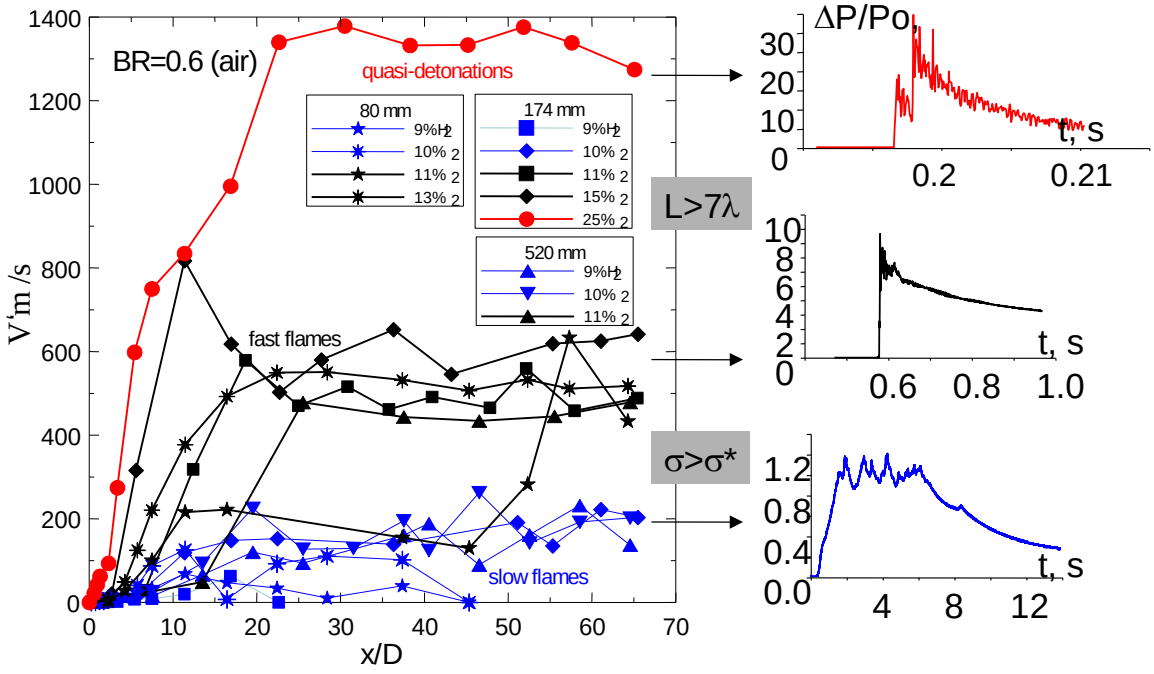

Figure 26. Combustion regimes for different hydrogen-air mixtures (P = 1 bar, T = 293K): right pictures correspond to pressure signals for different regimes (Dorofeev et al., 2001, 2000).

As it was suggested by Dorofeev and co-authors, expansion rate σ* (Dorofeev et al., 2001) and 7λ criteria (Dorofeev et al., 1997, 2000) can be considered as potentials of strong flame acceleration and detonation onset correspondingly. Mixtures with the expansion rate σ above the critical value σ* can effectively accelerate and then detonate, if the detonation criteria $L > 7\lambda$ is satisfied (L is the characteristic size of the combustible domain, λ is the detonation cell size). The mixtures with $\sigma < \sigma^*$ can not accelerate effectively and a subsonic combustion regime may only occur. Characteristic pressure load from the combustion

process is a function of combustion regime and can change from 1-2 bar for slow combustion, to 6-8 bar for sonic flames and 20-40 bar for detonation for initial pressure 1 bar (see Figure 26).

The objective of this part is to evaluate the critical conditions for flame acceleration and detonation transition for hydrogen-air mixtures at cryogenic temperatures, possibly in the presence of condensed oxygen and nitrogen. The data are required for safety analysis to evaluate the strongest possible combustion pressure and safety distances for LH2 explosions.

4.2.1. Flame acceleration limit. Critical expansion ratio.

The critical expansion ratio σ* is a function of dimensionless integral scale as Peclet number Pe = L_T/δ (L_T - turbulent length scale, δ -laminar flame thickness) and Zeldovich number β (β = $E_a(T_b-T_u)/T_b^2$). The critical expansion ratio σ* decreases with initial temperature T_u increase and overall energy activation E_a decrease (see the Figure 27). Dorofeev et al. (2001) give a polynomial correlation to evaluate the critical expansion ratio as a function of temperature

$$\sigma^* = 9.0\cdot10^{-6}x^3 - 0.0019x^2 + 0.1807x + .2314,$$

where $x=E_a/RT_u$. Assuming a constant activation energy E_a=7500K for hydrogen-air mixtures in wide range of temperatures and concentrations, an extrapolation to cryogenic temperatures gives the values of the critical expansion ratio σ* = 7.89 at T = 80K and σ* = 6.9 at T = 100K. It corresponds roughly to 7-8%H2 in air. The assumption about the constant activation energy in wide range of temperatures and concentrations is very strong and may lead to over-conservative results by shifting the critical concentration to leaner hydrogen – air mixtures which requires stronger measures to the hydrogen safety.

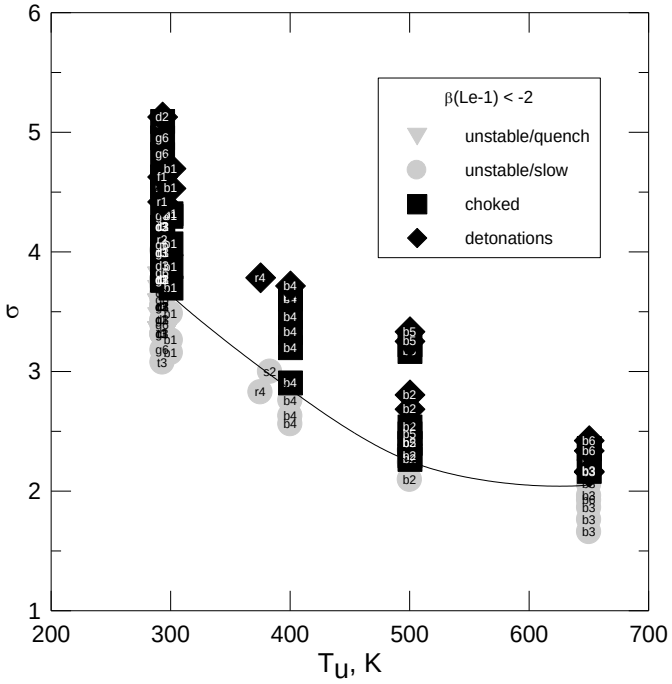

Figure 27. Resulting combustion regime as a function of critical expansion ratio σ and initial temperature T_u for hydrogen – air mixtures: black points – fast; gray points - slow combustion regimes (Dorofeev et al., 2001).

Figure 28 shows an extrapolation of critical expansion ratio to cryogenic temperatures. Far extrapolation to low temperatures gives the values of critical expansion ratio σ* at different initial temperatures (Figure 28). Table 5 also gives the critical bounding hydrogen concentration for an effective flame acceleration to the speed of sound or even higher velocity and detonations. It follows from the data that the lower hydrogen concentration for FA to speed of sound reduces from 11 to 9.6%H2 (σ* = 8.5) with temperature decrease from 300K to 100K and to 9.1%H2 (σ* = 10.7) with temperature decrease to 78K.

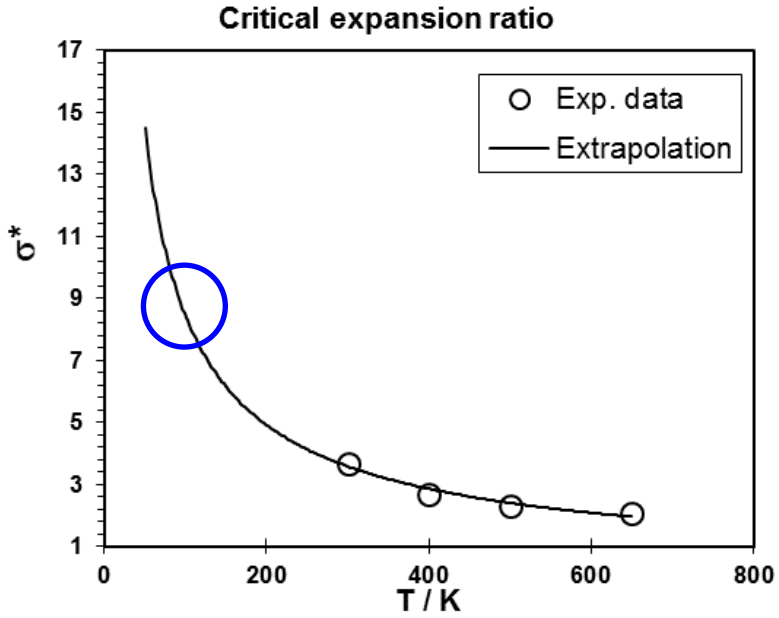

Figure 28. Critical mixture expansion ratios versus initial temperature (Dorofeev et al., 2001): extrapolation to cryogenic temperatures (solid line). Blue circle indicates the point of interest at cryogenic temperatures.

Table 5 Extrapolated temperature dependence on critical expansion ratio

T, K	C_{H2}, %mol	σ*
300	11	3.75
200	10.34	4.92
150	10.09	6.14
100	9.58	8.49
78	9.13	10.67
50	8.60	13.89

The previous extrapolation looks not confident enough because it is too far for such nonlinear dependence. Dependence of critical expansion ratio vs. Zeldovich number looks more linear (Figure 29). Assuming the constant activation energy, an effect of initial temperature on the critical expansion ratio can also be evaluated. Extrapolation to cryogenic temperature 80K leads to Zeldovich number increase from 5 to 11. According to the

correlation in Figure 29, it corresponds to the critical expansion ratio of about $\sigma^* = 8$, which in turn corresponds to 7%H2/air mixture at 80K. This value looks more reasonable and confident to be used as a first assumption before forthcoming PRESLHY experiments.

Due to the very far extrapolation of existing experimental data (no experimental data for temperatures below 273-293K), there is a highly requested need to experimentally check the theoretical prediction of critical expansion ratio at cryogenic temperatures. Another reason is that independent of the very high thermodynamic potential of combustion at cryogenic temperatures caused by three times higher density, the chemical reactivity of such compositions as 7% H2/air at low temperatures might be too low even to be ignited.

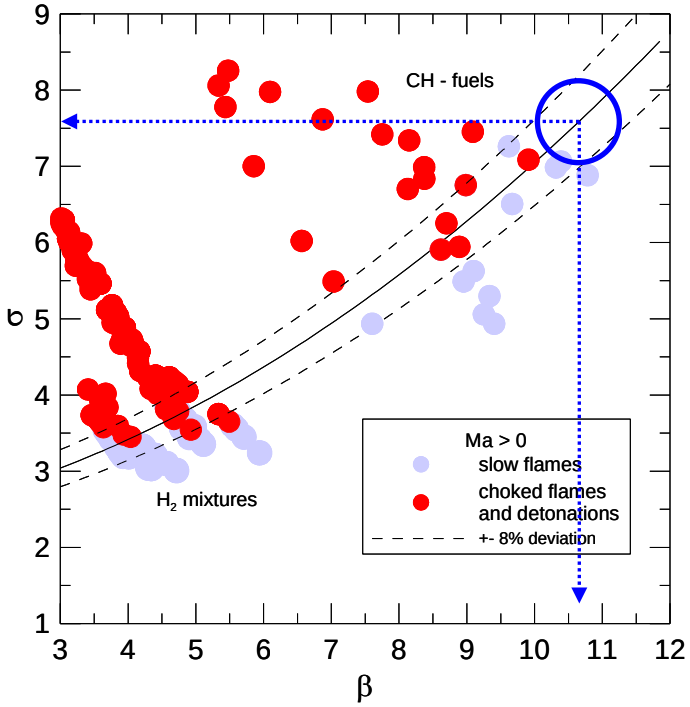

Figure 29. Critical mixture expansion ratios for possible development of fast flames in obstructed channels vs. Zeldovich number (Dorofeev et al., 2001). Blue circle indicates the point of interest extrapolated to cryogenic temperatures.

4.2.2. Deflagration to Detonation Transition (DDT) and Detonation.

As Figure 26 shows, the detonations may only occur if the flame is able to reach the speed of sound. Then, the critical condition when the characteristic dimension of the channel (diameter of the tube, for instance) $L > \lambda/\pi$ for a smooth channel or $L > 7\lambda$ for an obstructed channel should be satisfied (Dorofeev et al., 2000). This means that the characteristic size of the combustible system should exceed seven cell sizes for detonation onset inside of the obstructed channel.

There is a lack of experimental data on detonation cell size at cryogenic and reduced (lower than normal) temperatures in mixtures containing hydrogen. Only one reference is known regarding this low temperature problem. The paper of Zitoun et al. (1995) gives detonation cell sizes for stoichiometric hydrogen oxygen mixtures at 123K and different initial pressures (see Table 6).

Table 6 Detonation cell sizes for stoichiometric hydrogen – oxygen mixtures at reduced (cryogenic) temperatures

Temperature, T (K)	Pressure, p (bar)	Detonation cell width, λ (mm)
123	0.4918	1.4819
123	0.6953	0.9901
123	0.9827	0.6889

For hydrogen-air mixtures we only have experimental data on the influence of elevated initial temperature on detonation cell size (see Figure 30). In general, in accordance with referred data of Tieszen et al. (1987) and Stamps and Tieszen (1991) the detonation cell size is increasing with temperature decrease. These referred data are covered relatively narrow range of temperatures (278-373K) for hydrogen-air mixture with $\phi = 0.5$. In general, we can extrapolate these data to lower temperatures but not far. The best way to resolve this problem is to compute using CELL_H2 for detonation cell calculations (Gavrikov et al., 2000). The code CELL_H2 is using different chemical kinetic models and multidimensional detonation cell structure assumption and verified in wide range of elevated pressures and temperatures and mixture compositions. It demonstrates very good capability within the range 278-373K. The most problem is low temperature limitation of the CELL_H2 code below 200 K due to the 200 K limit of available range of thermodynamic and kinetic properties. It follows from Figure 31 that the CELL_H2 code demonstrates not so good reliability as for elevated and normal temperatures (Tieszen et al., 1987; Stamps and Tieszen, 1991; Denisov and Troshin, 1960) to be used for cryogenic temperatures for hydrogen-oxygen mixtures (Zitoun et al. (1995). Thus, the CELL_H2 code gives strong under-prediction compared to the experimental data (Zitoun et al. (1995). However, Figure 30 and Figure 31 demonstrate that until maximum of the dependence λ(T) and even to beginning of the decay at temperatures lower than 273K the code gives proper results.

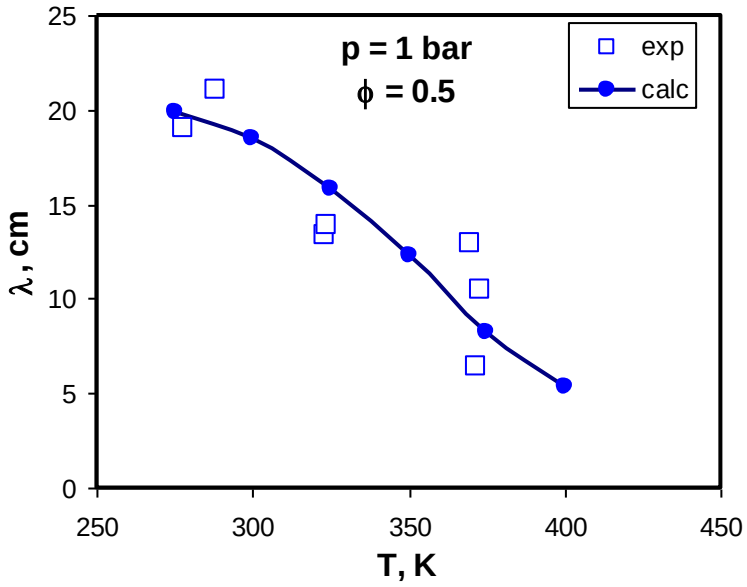

Figure 30. Comparison of calculated and experimental Tieszen et al. (1987) and Stamps and Tieszen (1991) detonation cell size data for hydrogen-air mixtures at different temperatures (p = 1 bar)

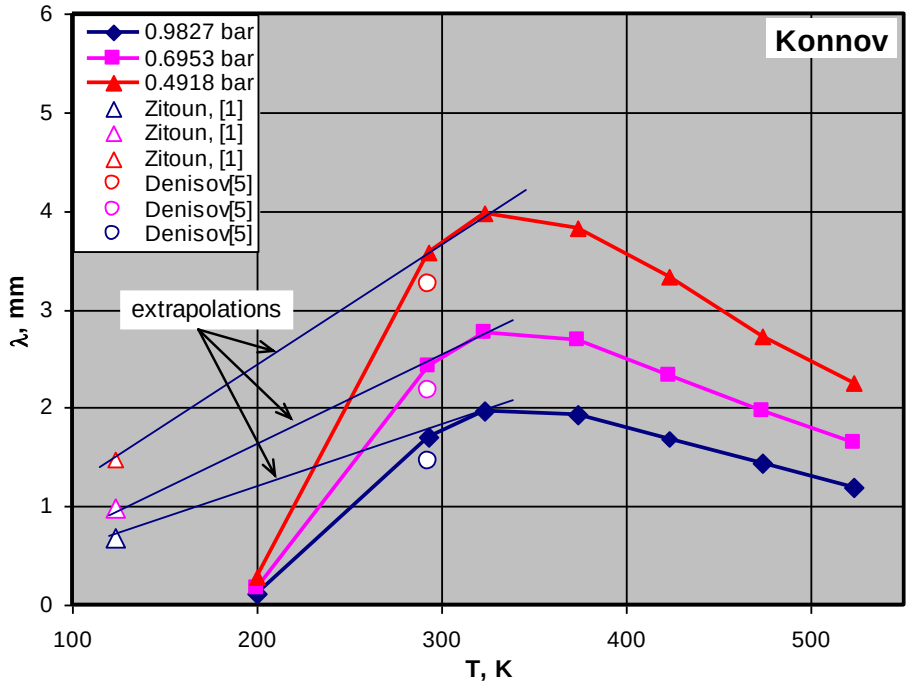

Figure 31. Comparison of calculated and experimental detonation cell size data for hydrogen-oxygen mixtures at different temperatures and pressures

Figure 32 explains an attempt to calculate the detonation cell sizes at low temperatures for hydrogen air mixtures. In general, the detonation cell size slightly increases with initial temperature decrease. Then, after it reaches the maximum, the dependence goes down too rapid as compared with low temperature experiments (Zitoun et al. (1995). As shown in Figure 31, the tangent at the maximum might be extrapolated to 100K to get more reliable data than the linear extrapolation directly from high temperature domain. Our evaluation of detonation cell sizes for three different hydrogen-air compositions at different temperatures is given in Table 7.

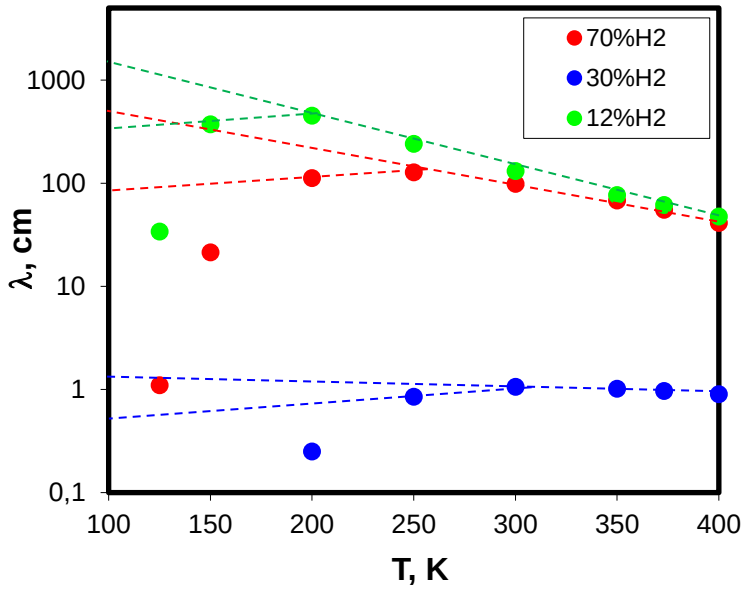

Figure 32. Comparison of calculated and experimental detonation cell size data for hydrogen-oxygen mixtures at different temperatures and pressures

The confidence of proposed extrapolation is very low. With the lack of experimental data on detonation cell sizes for hydrogen-air mixtures at cryogenic temperatures, it needs additional experiments on detonation cell size measurements.

Table 7 Detonation cell sizes for different hydrogen – air mixtures at reduced temperatures (P = 1bar)

Temperature, T (K)	Detonation cell width λ, cm		
	Hydrogen concentration, %vol.		
	12	30	70
373	61	0.97	55
300	131	1.06	99
250	240	0.85	127
200	450	0.79	112
150	372	0.63	100
100	316	0.50	79

4.2.3. Concluding remarks

This section can be summarized as follows:

- There is no experimental data on the critical expansion ratio for hydrogen-air compositions at initial temperatures less than 273K.
- Due to the very far extrapolation of existing experimental data (no experimental data for temperatures below 273-293K), there is a highly requested need to experimentally check the theoretical prediction of critical expansion ratio at cryogenic temperatures. Another reason is that independent of the very high thermodynamic potential of combustion at cryogenic temperatures caused by three times higher density, the chemical reactivity of such compositions as 7% H2/air at low temperatures might be too low even to be ignited.
- The confidence of the proposed extrapolation is very low. With the lack of experimental data on detonation cell sizes for hydrogen-air mixtures at cryogenic temperatures, it needs additional experiments on detonation cell size measurements.
- Shock tube experiments should be used for experimental investigation of FA and DDT conditions for hydrogen-air mixtures at cryogenic temperatures.

4.2.4. References

Denisov, Yu.N. and Ya.K. Troshin. Structure of gaseous detonation in tubes. Sov. Phys. Tech. Phys., 5(4):419-431, 1960.

Dorofeev S. B., M. S. Kuznetsov, V. I. Alekseev, A. A. Efimenko, and W. Breitung. Evaluation of limits for effective flame acceleration in hydrogen mixtures. J. Loss Prev. Proces. Ind., 14, 583 (2001).

Dorofeev S., V. Sidorov, A. Dvoinishnikov, A. Denkevits, A. Efimenko, and A. Lelyakin. Large Scale Hydrogen-Air-Steam DDT Experiments in the RUT Facility. Test Series 1996. RRC KI 80-05/16 (1997).

Dorofeev S.B., Sidorov V. P., Kuznetsov M. S., Matsukov I. D., Alekseev V. I. Effect of scale on the onset of detonations. Shock Waves, V. 10, pp. 137-149 (2000)

Eric BAVOIL Etude expérimentale de l'influence de la diminution de la température initiale (jusqu'à 100K) sur les déflagrations des mélanges H2-air Université de Poitiers (1997)

Gavrikov A.I., A.A. Efimenko, and S.B. Dorofeev, Detonation cell size predictions from detailed chemical kinetic calculations. Combustion and Flame 120: 19-33 (2000).

Goodwin, D.G., Cantera User's Guide, California Institute of Technology, Pasadena, CA, November, 2001

Lutz, A.E.. Sandia A numerical study of thermal ignition. Technical Report SAND88-8228, Sandia National Laboratories (1988)

Reynolds W.C., The Element Potential Method for Chemical Equilibrium Analysis: Implementation in the Interactive Program STANJAN Version 3, Dept. of Mechanical Engineering, Stanford University, Palo Alto, California, January 1986 (1986)

Stamps D.W. and S.R. Tieszen. The influence of initial pressure and temperature on hydrogen-air-diluent detonations. Combust. Flame, 83(3):353-364, 1991.

Tieszen, S.R., M.P. Sherman, W.B. Benedick, and M. Berman. Detonability of H_2-air-diluent mixtures. Technical Report NUREG/CR-4905, SAND85-1263, Sandia National Laboratories, 1987.

Zabetakis M.G. and Burgess D.S, 1961, "Research in Hazards Associated with the Production and Handling of Liquid Hydrogen", US Bureau of Mines Report, RI5707

Zitoun, R., D. Desbordes, C. Guerraud, and B. Deshaies. Direct initiation of detonation in cryogenic gaseous H_2-O_2 mixtures. Shock Waves, 4(6):331-337, 1995.

4.3. Flame propagation over a spill of LH2 (KIT)

There are two scenarios associated with a combustion of a liquid hydrogen spill: a stationary pool fire, a flame propagation over a spill of LH2 in the case of late ignition. The first scenario is based on the energy balance between flame and surface of the liquid hydrogen. The layer thickness should be large enough to avoid an effect of heat transfer from the ground to bulk LH2.

The scheme of energy balance for LH2 – pool fire is shown in Figure 33. The heat flux for heating and evaporating of liquid hydrogen under stationary combustion q_0 is determined by the expression:

$$q_o = \rho \cdot u \cdot (c_p \cdot \Delta T_b + r) = q_{oT} + q_{or}, \qquad (21)$$

where u is the linear rate of liquid fuel burnup, $\Delta T_к = T_b - T_o$, T_b is the boiling temperature; r is the specific heat of vaporization. The heat flux q_o should be delivered by flame radiation to the evaporating surface of LH2 to support stationary pool fire. Up to now, there is no data on stationary LH2 pool fire linear rate. The values of q_o and u are incognita and should be experimentally measured.

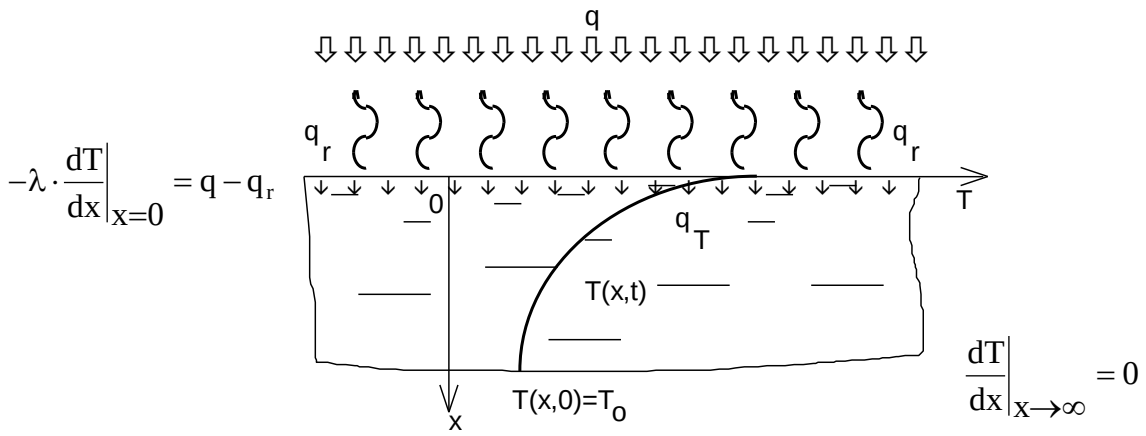

Figure 33. The scheme of heat transfer from gaseous flame to LH2 surface. q_r and q_T are the heat flux spent for LH2 evaporation and to heat up the LH2 layer to proper evaporation; λ is the thermal conductivity of the LH2; To is the bulk temperature of LH2.

The theory of stationary pool fire was developed for industrial fossil fuels and then extended to hydrogen. According to the work of Hottel (1958), Zebatakis (1967) and Babraukas (1983), equations for predicting the regression rate of pool fire are proposed in the literature. The following Figure 34 and Table 8 present the main characteristics of pool fires for LH_2, LNG and gasoline.

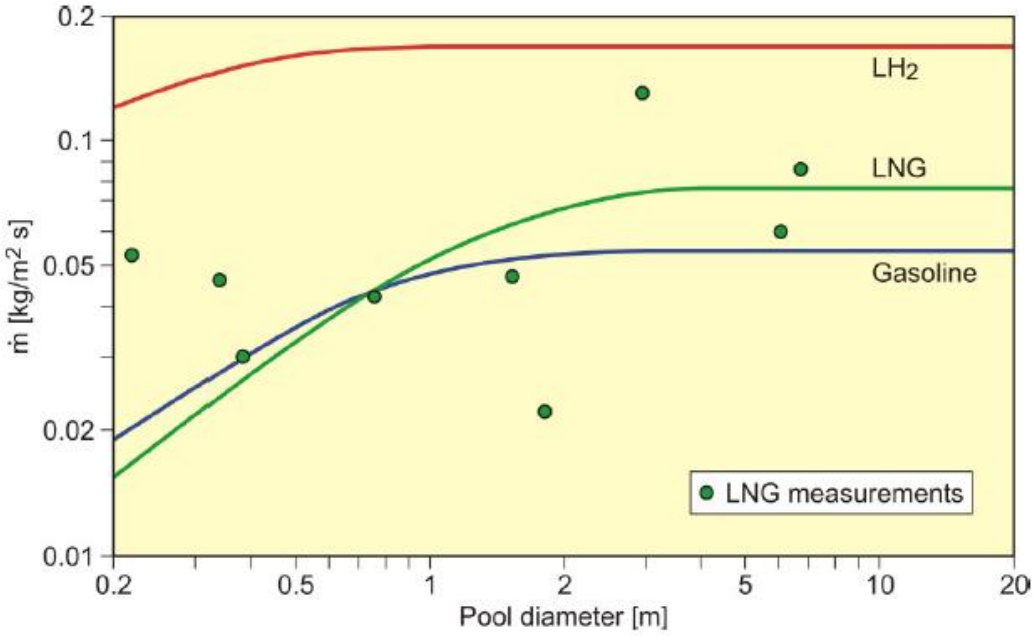

Figure 34. Stationary burning rates for different liquid fuels. LH2 data extrapolated (Babraukas, 1983).

Table 8 Characteristics of pool fire for different liquid fuels

Fluid	Density [kg/m^3]	ΔH_v [kJ/kg]	ΔH_c [MJ/kg]	k β $^{(1)}$ [m^{-1}]	T_f $^{(1)}$ [K]	$\dot{m}_\infty$ $^{(2)}$ [mm/min]	$\dot{v}_\infty$ $^{(3)}$ [mm/min]
LH_2	71	446	120	6.1	1600	142.2	20.5
LNG	422	510	61	1.1	1500	11.1	9.1
LPG	544	428	46	1.4		10.9	8.2
Gasoline	737	330	44	2.1	1450	4.5	11.3

The classical equation of heat balance for pool fire (Eq. 21) assumes stationary boundary conditions as shown in Figure 33 and can be easily realized for gasoline LPG and even LNG. It should be a rather thick layer of liquid fuel and relatively long exposure time to establish the condition dT/dx = 0 at a far distance from the surface. For LNG and for LH2 during an accident the process is highly instationary and more close to flush evaporation and rapid phase transition. For such process the heat transfer coefficient is of the order (100 – 1000) W/(m^2 K). Then, the heat flux from solid surface to liquid hydrogen is about (30 – 300) kW/m^2. For instance, direct measurements of the evaporation rate of LH2 above the concrete surface give the values 0.6 – 3.3 kW/m^2 (Takeno et al., 1994). It fits very well to theoretical calculations of 1.7-2.1 kW/m^2. Due to this fact, the contribution of heat radiation of LH2 pool fire (1 – 10) kW/m^2 (Schefer at al., 2007; Panda and Hecht, 2017; Friedrich et al. 2012) to the combustion process is negligibly small compared to heat flux from solid surface to LH2. So that the LH2 pool fire is fully controlled by heat transfer from solid material to LH2. This means that the measurements of evaporation rate due to heat transfer from the warm ground surface (sand, concrete, ground) is of great importance for the current PRESLHY project.

Since the evaporation rate really controls the LH2 pool fire, the geometry of such flame and Surface Emissive Power (SEP) should be a function of heat transfer from different materials to LH2. In case of late ignition of hydrogen cloud formed due to the flush evaporation and rapid phase transition, the flame propagation in a semiconfined cloud above LH2 pool should also be investigated.

4.4. LH2 combustion with congestion/confinement variation

The problem of LH2 combustion with congestion/confinement is relevant to ‘realistic’ liquid hydrogen releases from LH2 – jet/plume/pool into open/semi-open congested or non-congested space and then combustion of cold non-uniform hydrogen-air mixture in congested partially confined environment. The problem is manifold. It considers the flame propagation in presence of concentration stratification and an influence of geometrical non-uniformities such as obstruction rig and solid interfaces such as ground/floor or sidewalls.

In the current PRESLHY project, the HSL specifies the geometry as shown in Figure 35. The system consists of a hydrogen cloud mixed with air above the LH2-pool as a continuous source of hydrogen (Figure 35, left) or LH2 jet/plum released to air atmosphere. The cloud above LH2-pool and LH2-hydrogen jet cloud penetrate through a metal construction as an obstruction rig for more efficient flame acceleration and to reach a faster combustion regime within a shorter distance.

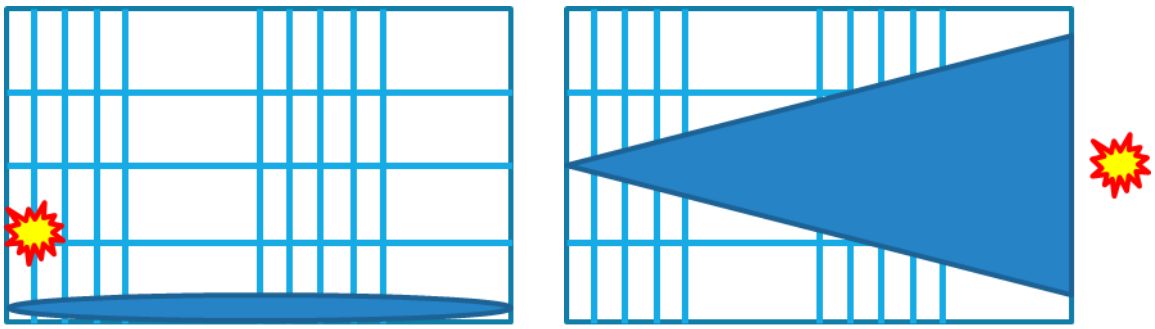

Figure 35. Geometry of gaseous cloud in the cases of cryogenic hydrogen combustion above the LH2-pool (left) or in the case of LH2 jet/plume release in air (right)

Figure 36 shows the nature of the hydrogen cloud above the spill of liquid hydrogen. Under conditions of natural convection and diffusion, the cloud has a zero hydrogen concentration and ambient temperature on top of the cloud and pure hydrogen concentration and T_L = 20.3K above the LH2 surface. With respect to the combustion process of such non-uniform cloud, the only concentration range between 4 and 75%H2 is of practical interest. Within the flammable range (4-75%H2), assuming a linear concentration gradient, an equilibrium temperature theoretically changes from 273 to 75K, respectively. In reality, the flammable range of hydrogen concentrations shrinks from 4 to 70%H2 taking into account the air condensation at lower cryogenic temperatures. Then, the mixture should be ignited at the position of the highest hydrogen reactivity (30%H2) to measure possible flame propagation velocity with and without obstacles. A point ignition source or linear igniter might be used to ignite the cloud.

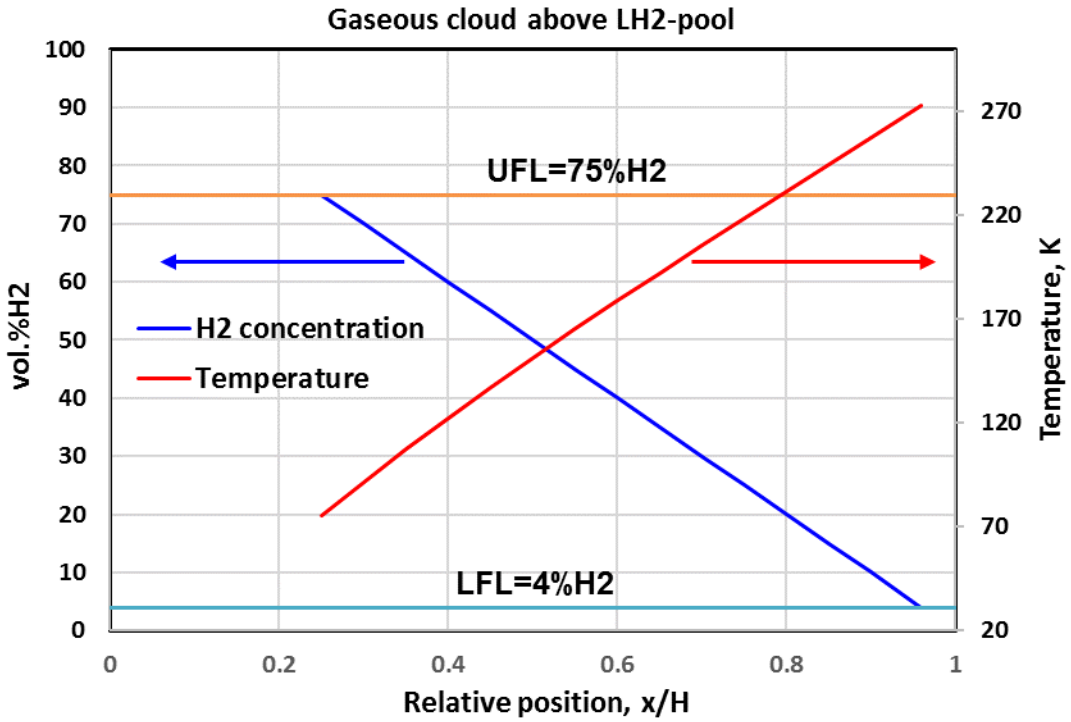

Figure 36. The structure of stratified hydrogen cloud above a LH2 spill.

Such a system is very similar to that dedicated to study flame propagation regimes in a stratified semiconfined layer of hydrogen-air mixture (Kuznetsov et al., 2011, Kuznetsov et al., 2015; Grune et al., 2017) with a difference that it will be an inverse stratification of hydrogen above the LH2-pool with higher hydrogen concentration at the bottom compared to natural stratification at ambient temperature with the higher hydrogen concentration at the top. Another difference is that it will also be a temperature gradient depending on local hydrogen concentration as shown in Figure 40. Hydrogen distribution in an obstructed layer: (a) by varying of the hydrogen concentration in a mixing tank; (b) by pressure changing in a mixing tank (Kuznetsov et al., 2015b).

All critical conditions for the current system have to be quite similar to that for the natural stratified layer with an effect of inverse hydrogen concentration gradient, gravity and presence of temperature non-uniformity.

A number of experiments and numerical simulations have been done with respect to combustion and detonation in a semiconfined stratified or uniform layer of hydrogen-air mixture typical for accident scenario in a containment of nuclear reactor or in a tunnel geometry. Experiments on hydrogen combustion in a thin semiconfined layer have been performed inside the safety vessel with a volume of 100 m^3 (Kuznetsov et al., 2011, 2015). A rectangular box with dimensions of 9 x 3 x 0.6 m was installed inside the safety vessel of 100 m^3 volume.

All experimental data on characteristic pressures and flame velocities for uniform compositions are summarized in Figure 37. The figure shows that in semi-open channel experiments the threshold between the slow and fast flame regimes is the sonic speed in reactants c_r, while in closed channels it is the sonic speed of the products (Alekseev et al., 2001). Figure 37 demonstrates that the thinner is the layer thickness, the higher the hydrogen concentration or more reactive mixture has to be to reach the speed of sound.

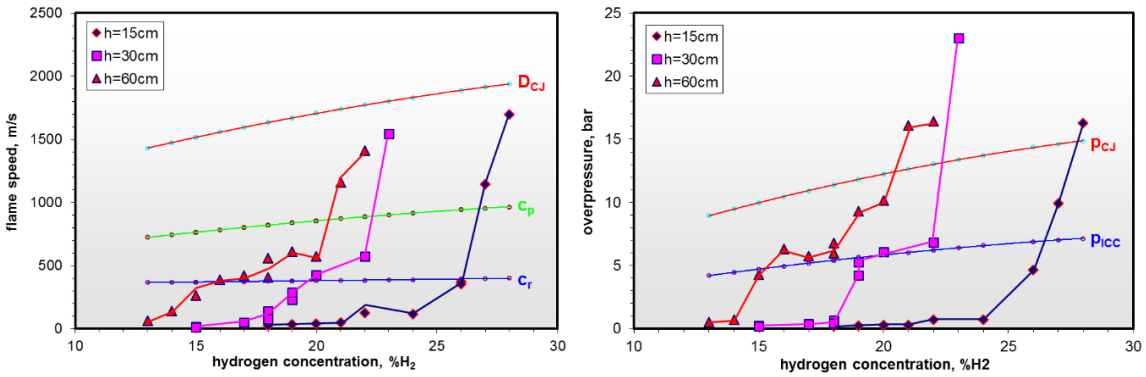

Figure 37. Characteristic flame velocity and overpressure for different layer thicknesses as function of hydrogen concentration: Here cr, cp, DCJ are sonic speed in reactants, products and CJ-detonation velocity; pICC and pCJ are adiabatic isochoric complete combustion pressure and CJ-detonation pressure (Kuznetsov et al., 2011).

In terms of hydrogen concentration and critical expansion ratio σ*, the critical conditions for fast sonic flames for different layer thickness are the following (see Figure 37):

$$h = 0.15 \text{ m for } 26\% \text{ } H_2 \quad (\sigma^* > 4.63) \tag{22}$$

$$h = 0.3 \text{ m for } 19\% \text{ } H_2 \quad (\sigma^* > 5.42) \tag{23}$$

$$h = 0.6 \text{ m for } 15\% \text{ } H_2 \quad (\sigma^* > 6.6) \tag{24}$$

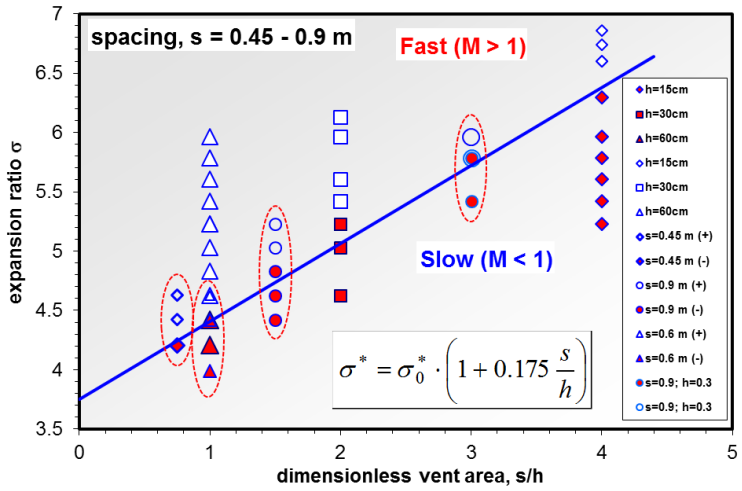

Figure 38. Critical conditions for an effective flame acceleration as function of expansion ratio vs. dimensionless vent area: sonic flame and detonations (open points); subsonic flame (solid points). Different spacing between obstacles is also shown (Kuznetsov et al., 2011).

Since expansion ratio is a critical indicator of the potential for flame acceleration (Dorofeev et al., 2001; Alekseev et al., 2001), Figure 38 summarizes all experiments as a dependence of expansion ratio versus layer thickness and spacing between obstacles for the semi-confined layer. A linear correlation between the critical expansion ratio σ* for fast flame propagation in a flat layer and the reciprocal layer thickness 1/*h* or spacing between the obstacles, *s*, was derived from the experiments (Figure 38) and theoretical considerations:

$$\sigma^* = \sigma_0^*(1+K\cdot s/h), \quad (25)$$

where $\sigma_0^* = 3.75$ is the critical expansion for hydrogen-air mixtures in an enclosure; K = 0.175 is a constant depending on the blockage ratio (BR = $1 - d^2/D^2$, where *d* is the orifice diameter; *D* is the channel cross-section). The ratio $\alpha = s/h$ can be an equivalent of vent ratio for the system with a lateral venting as a channel with a side venting (Alekseev et al., 2001). Then, the condition for fast flame acceleration looks quite similar:

$$\sigma^* = \sigma_0^*(1+2\cdot\alpha), \quad (26)$$

This means that for a channel with 50% side venting it should be a mixture with expansion ratio σ* = 7.5 (almost the same as a stoichiometric hydrogen-air mixture) to be able to accelerate to the speed of sound and then to detonate.

According to Kuznetsov et al. (2011), the detonation for uniform hydrogen-air compositions occurs at different hydrogen concentration depending on the layer thickness (Figure 37):

$$h = 0.15 \text{ m for } 27\% H_2, \quad (27)$$

$$h = 0.3 \text{ m for } 23\% H_2, \quad (28)$$

$$h = 0.6 \text{ m for } 21\% H_2, \quad (29)$$

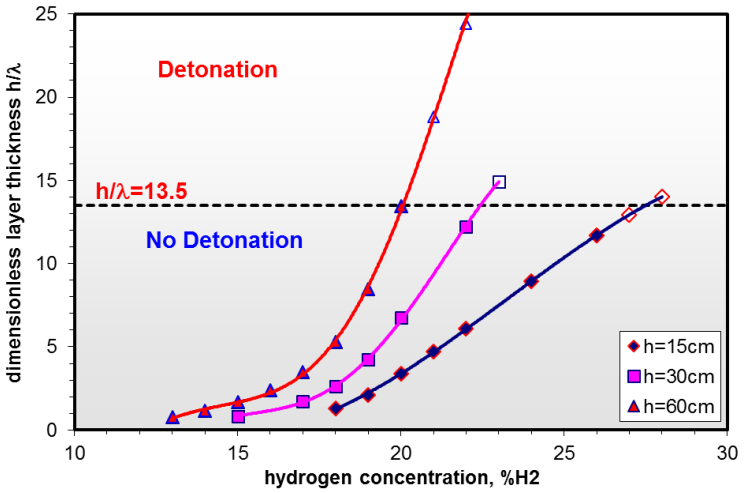

Figure 39. Critical conditions for DDT in the relationship between the dimensionless layer thickness and hydrogen concentration: detonation (open points); no detonation (solid points) (Kuznetsov et al., 2011).

The thinner layer needs a more reactive mixture to be detonated than a thicker one. Since the energy losses and the mixture reactivity are reciprocally correlated with layer thickness and detonation cell width λ, the dimensionless ratio of the layer thickness over the detonation cell width h/λ is expected to be a constant value for the critical detonation conditions. Figure 39 confirms that the critical dimensionless layer thickness h/λ for detonation onset is almost the same for three investigated layer thicknesses (Kuznetsov et al., 2011).

An effect of different linear hydrogen concentration gradients of 0.2, 0.3 and 0.6%H_2/cm has been investigated inside a thin layer box by using an effect of turbulent diffusion during the gas injection (Kuznetsov et al., 2015). Figure 40 shows an example on the formation of a linear concentration gradient by varying the mixture composition at constant pressure (Figure 40a) or changing of initial pressure in a mixing tank at the same hydrogen concentration (Figure 40b).

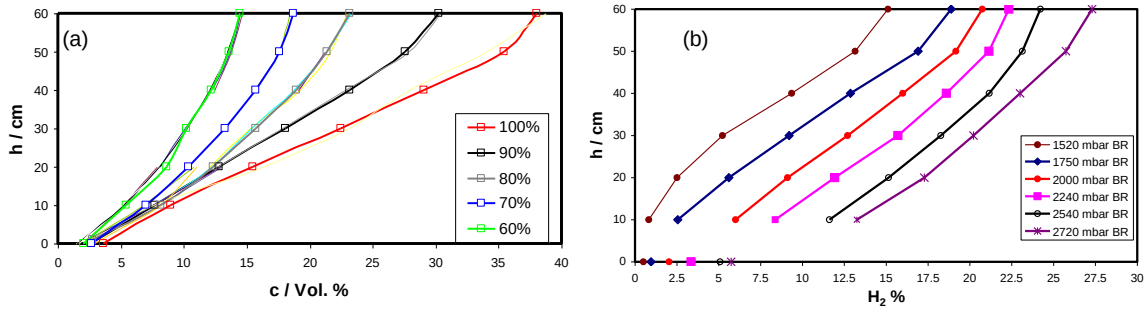

Figure 40. Hydrogen distribution in an obstructed layer: (a) by varying of the hydrogen concentration in a mixing tank; (b) by pressure changing in a mixing tank (Kuznetsov et al., 2015b).

Because experiments demonstrate almost no influence of hydrogen stratification on critical conditions for flame acceleration, formula (Eq. 24) to evaluate the critical expansion ratio in the stratified atmosphere remains the same as for uniform compositions:

$$\sigma^* = \sigma_0^*(1+K\cdot s/h), \qquad (30)$$

where σ* is the critical expansion ratio for maximum hydrogen concentration at the ceiling of the channel. Except for the highest gradient of 0.6%H_2/cm, there is almost no influence of the gradient on flame propagation velocity for stratified compositions. The process of combustion in a stratified atmosphere is governed by the maximum hydrogen concentration at the ceiling of the channel. Then, the critical conditions for DDT in a stratified atmosphere remain the same as in Eq. 29 with the difference that for stratified atmosphere efficient layer thickness *h** should be evaluated up to the lower detonable hydrogen concentration of 13-14%H_2 (Grune et al., 2017):

$$h^*/\lambda = 13\text{-}14 \qquad (31)$$

where *h** is the efficient height of the detonable layer of the hydrogen-air mixture; λ is the detonation cell size of hydrogen-air mixture at the ceiling.

As Figure 37 shows, the maximum combustion pressure or strength of shock wave depends on flame propagation regime and flame velocity. Figure 41 demonstrates the dependence of maximum combustion pressure on flame propagation velocity in a semi-confined stratified layer geometry. Approaching the flame speed to the speed of sound (M=1) leads to maximum combustion over-pressure ΔP_{max} > 4-5 bar. The low reactivity of hydrogen-air mixture, low blockage or no obstructions, unconfined geometry can lead to very low flame propagation velocity. Then, the resulting combustion over-pressure may not exceed the level of 1 bar.

Within the current PRESLHY project, we may expect a confirmation of no influence of inverse stratification for the cryogenic cloud on critical conditions for different flame propagation regimes compared with natural stratification at ambient conditions. At least the difference should not be very significant because characteristic local temperature corresponding to stoichiometric hydrogen-air mixture occurs at 205.6K, not so low as cryogenic temperatures at the pool surface T_L = 20.3K. However, the influence of the temperature gradient should be carefully investigated.

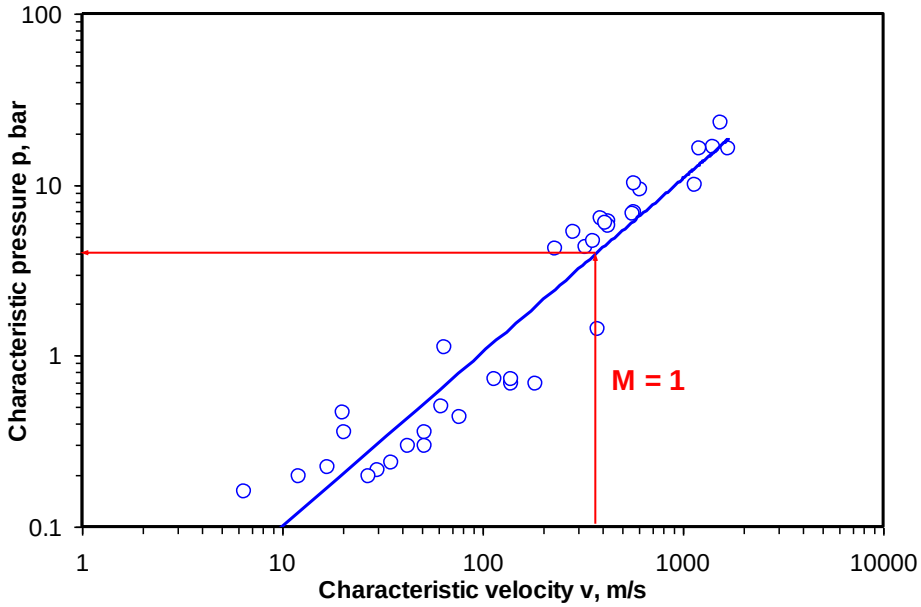

Figure 41. An effect of flame propagation velocity on maximum combustion pressure in a thin semi-confined layer geometry (Kuznetsov et al., 2011).

4.1. Concluding remarks

- Since the evaporation rate really controls the LH2 pool fire, the geometry of such flame and Surface Emissive Power (SEP) should be a function of heat transfer from different materials to LH2. Then, the pool fire, its dimension and thermal radiation as a function of heat transfer from different materials and evaporation rate should be experimentally investigated.
- In case of the late ignition of hydrogen cloud formed due to the flush evaporation and rapid phase transition, the flame propagation in a semiconfined cloud above LH2 pool should also be investigated.
- Within the current PRESLHY project, we may expect a confirmation of no influence of inverse stratification for the cryogenic cloud on critical conditions for different flame propagation regimes compared with natural stratification at ambient conditions. At least the difference should not be very significant because characteristic local temperature corresponding to stoichiometric hydrogen-air mixture occurs at 205.6K, not so low as cryogenic temperatures at the pool surface T_L = 20.3K. However, the influence of temperature gradient inverse stratification on flame propagation regimes and maximum combustion pressure should be investigated.

5. References

Alekseev, V.I., Kuznetsov, M.S., Yankin, Yu., G., Dorofeev, S.B. (2001) Experimental study of flame acceleration and DDT under conditions of transverse venting. J. Loss Prev. Proc. Ind., 14/6: 591-596.

Babrauskas, V. Estimating large pool fire burning rates. *Fire Technol* **19,** 251–261 (1983)

Dorofeev, S.B., Kuznetsov, M.S., Alekseev, V.I., Efimenko, A.A., Breitung, W. (2001) Evaluation of limits for effective flame acceleration in hydrogen mixtures. J. Loss Prev. Proc. Ind., 14 (6): 583-589.

Dorofeev, S.B., Sidorov, V. P., Kuznetsov, M. S., Matsukov, I. D., Alekseev, V. I. (2000) Effect of scale on the onset of detonations. Shock Waves, v. 10, pp. 137-149.

Friedrich, A., Grune, J., Jordan, T., Kotchourko, A., Kotchourko, N., Kuznetsov, M., Sempert, K., Stern, G. (2007a) Experimental study of hydrogen-air deflagrations in flat layer. In: Proc. 2nd ICHS International Conference on Hydrogen Safety. September 11 - 13, 2007 San Sebastian – SPAIN, paper 1.3.106, 1-12.

Friedrich, A., Grune, J., Kotchourko, N., Kotchourko, A., Sempert, K., Stern, G., Kuznetsov, M. (2007b) Experimental study of jet-formed hydrogen-air mixtures and pressure loads from their deflagrations in low confined surroundings. International Conference on Hydrogen Safety, San Sebastian, Spain, paper 1.3.125, 1-13

Gan Cui, Zili Li, Chao Yang, Zhen Zhou and Jianle Li Experimental Study of Minimum Ignition Energy of Methane–Air Mixtures at Low Temperatures and Elevated Pressures Energy Fuels, 2016, 30 (8), pp 6738–6744

Gasse A. Experimentelle Bestimmung und simulation von Explosiongrenzen, untersucht an wasserstoffhaltigen Brenngasgemischen. Dissertation Universitдt-Gesamthochschule Paderborn, Reihe Verfahrenstechnik, Shaker, Aachen (1992)

Grune, J., Sempert, K., Kuznetsov, M., Breitung, W. (2011) Experimental study of ignited unsteady hydrogen jets into air. International Journal of Hydrogen Energy, vol. 36, pp. 2497-2504.

Grune, J., Sempert, K., Kuznetsov, M., Jordan, T. (2014) Experimental study of ignited unsteady hydrogen releases from a high pressure reservoir. International Journal of Hydrogen Energy 39, 6176-6183.

Grune, J., Sempert, K., Friedrich, A., Kuznetsov, M., Jordan, T. (2017) Detonation wave propagation in semi-confined layers of hydrogen–air and hydrogen–oxygen mixtures. International Journal of Hydrogen Energy, Volume 42, Issue 11, 7589-7599.

Hottel, H.C., Certain Laws Governing Diffusive Burning of Liquids, Fire Research Abstracts and Reviews, Vol. 1, 1958, pp. 41–44.

Hubert Yves Rico Etudes théorique et expérimentale de la détonation des mélanges d'hydrogène liquide et d'oxygène solide à 20 K Thèse de doctorat de l'Université de Paris 1970.

Hustad J.E., Sonju O.K. Experimental studies of lower flammability limits of gases and mixtures of gases at elevated temperatures. Combust. Flame 71:283 (1988)

International Electrotechnical Commission, Electrical apparatus for explosive gas atmospheres - Part 20: Data for flammable gases and vapours, relating to the use of electrical apparatus, Standard IEC 60079-20:2000

Karim G.A., Wierzba I., Boon S. The lean flammability limits in air of methane, hydrogen and carbon monoxide at low temperatures. Cryogenics, 24(6), 1984, pp.305–308

Kumar R.K. Flammability limits of hydrogen-oxygen-diluent mixtures. AECL-8890. Journal of Fire Sciences, 3:235-262 (1985)

Kuznetsov M., Czerniak M., Grune J., Jordan T., Effect of temperature on laminar flame velocity for hydrogen-air mixtures at reduced pressures. Proc. of the 5th International Conference on Hydrogen Safety, ICHS 2013 September 9-11, 2013 - Brussels – Belgium, paper 231, p. 1-12

Kuznetsov, M. and Grune, J. (2019) Experiments on combustion regimes for hydrogen/air mixtures in a thin layer geometry. International Journal of Hydrogen Energy, 44 (7): 8727-8742.

Kuznetsov, M., Alekseev, V., Matsukov, I. (2002) Deflagration-to-Detonation Transition in H_2 -Air and H_2 -O_2 -N_2 mixtures in channels with obstructions. Advances in Confined Detonations (eds. G. Roy, S. Frolov, R. Santoro, S. Tsyganov), Torus Press Ltd., Moscow, pp 26-30.

Kuznetsov, M., Alekseev, V., Matsukov, I., Dorofeev, S. (2005) DDT in a smooth tube filled with a hydrogen–oxygen mixture. Shock Waves, 14: 205-215.

Kuznetsov, M., Friedrich, A., Stern, G., Kotchourko, N., Jallais, S., L'Hostis, B. (2015a) Medium-scale experiments on vented hydrogen deflagration. J Loss Prev Process Ind, 36:416-28.

Kuznetsov, M., Grune, J. (2019) Experiments on combustion regimes for hydrogen/air mixtures in a thin layer geometry. International Journal of Hydrogen Energy, 44 (7): 8727-8742.

Kuznetsov, M., Grune, J., Friedrich, A., Sempert, K., Breitung, W., Jordan, T. (2011) Hydrogen-air deflagrations and detonations in a semi-confined flat layer. In: Fire and Explosion Hazards, Proceedings of the Sixth International Seminar (Edited by D. Bradley, G. Makhviladze and V. Molkov), 125-136.

Kuznetsov, M., Lelyakin, A., Alekseev, V., Matsukov, I. (2017) Detonation transition in relatively short tubes. In: Ben-Dor G., Sadot O., Igra O. (eds) 30th International Symposium on Shock Waves 1. Springer Publ., 481-485.

Kuznetsov, M., R. Redlinger, Flammability limits of hydrogen-air and hydrogen-oxygen mixtures at elevated temperatures. 2nd quarter report, IceFuel Project, 2008

Kuznetsov, M., Yanez, J., Grune, J., Friedrich, A., Jordan, T. (2015b) Hydrogen combustion in a flat semi-confined layer with respect to the Fukushima Daiichi Accident. Nuclear Engineering and Design, 286: 36-48.

Kuznetsov, M.S., Alekseev, V. I., Dorofeev, S. B. (2000) Comparison of critical conditions for DDT in regular and irregular cellular detonation systems. Shock Waves, 10: 217-224.

Kuznetsov, M.S., Dorofeev, S. B., Efimenko, A. A., Alekseev, V. I., Breitung, W. (1997) Experimental and numerical studies on transmission of gaseous detonation to a less sensitive mixture. Shock Waves, vol. 7, 297-304.

Martín-Valdepeñas, J M, M A Jiménez, Exploring MIE as a Safety Indicator Parameter in Practical Applications, Universidad Politécnica De Madrid Escuela Técnica Superior De Ingenieros Industriales, Cátedra De Tecnología Nuclear, EU-Fifth Framework Programme (1998-2003), Contract EVG1-CT-2001-00042, EXPRO - Experimental and Numerical Study of Reactive Flows with Relevance to Industrial Safety for Explosion Protection, CTN-09/03, November 2003

National Aeronautics and Space Administration Report, Safety Standard for Hydrogen and Hydrogen Systems, Report NSS 1740.16, 1997, p. A-16.

Omar, M.H.; Z. Dokoupil Solubility of nitrogen and oxygen in liquid hydrogen at temperatures between 27 and 33°K Physica Volume 28 issue 5 1962

Richard W. High Some liquid oxygen / liquid hydrogen explosive effects in controlled failure mode tests NASA report 1969

Takeno, K., T. Ichinose, Y. Hyodo and H. Nakamura, Evaporation rates of liquid hydrogen and liquid oxygen spilled onto the ground. I. Loss Prev. Process Ind., 1994, 7(5): 425-431

Wierzba K. Harris G.A. Karim Effect of low temperature on the rich flammability limits in air of hydrogen and some fuel mixtures containing hydrogen International Journal of Hydrogen Energy Volume 17, Issue 2, February 1992, Pages 149-152

Zabetakis M.G. Flammability characteristics of combustible gases and vapors, Bureau of Mines Bulletin 627, p. 121 (1965)

Zabetakis, M. G. (1967). Safety with Cryogenic Fluids, Plenum Press, New York